PART IV

DRUG PRODUCTS

34

PROCESS MODELING TECHNIQUES AND APPLICATIONS FOR SOLID ORAL DRUG PRODUCTS

Mary T. am Ende, Rahul Bharadwaj, Salvador García-Muñoz, William Ketterhagen, and Andrew Prpich

Pharmaceutical Development, Pfizer Global Research & Development, Groton, CT, USA

Pankaj Doshi

Chemical Engineering and Process Division, National Chemical Laboratory, Pune, India

34.1 INTRODUCTION

The budget-restricted pharmaceutical environment is countered by the heightened expectations for drug products to be developed with more intensive use of science-based principles. The issues that arise during drug product development are often attributed to the impact of changing batch size, and equipment type or scale on the formulation and the process. In the commercial arena, one of the more prevalent causes for batch failures, or product not meeting specifications, is property shifts in the excipients or active pharmaceutical ingredient (API). During development and commercialization of a drug product, it is important to design a robust dosage form that is minimally sensitive to raw material variations and equipment scale.

The fundamental principles taught in the chemical engineering curriculum equip the chemical engineer with the skill base that allows them to address these complicated process operations and the understanding to connect the material properties to the processing equipment and design. Courses on the fundamental laws of heat transfer, mass transfer, momentum transfer, transport phenomena, and physical chemistry allow the chemical engineer to mathematically describe the process. For example, an impeller used to mix API and excipients imparts energy and momentum on the material to achieve uniformity of the blend. In this chapter, an example of powder discharging from a bin is monitored through computational methods to predict segregation. Utilizing the basics of the process calculations course enables students to break down the system into a control volume and solve mass and energy balances to determine the solution. An example of this type will be illustrated in this chapter during the derivation of the thermodynamic film-coating model. Process control principles allow the chemical engineer to develop models to accommodate variations in the inlet stream properties and can adjust the process through feedforward or feedback control to produce consistent quality product. In this chapter, this approach is used in reverse to set specifications on the raw material properties to ensure product quality using empirical models. The undergraduate curriculum, including many other courses not specifically highlighted in this chapter, provide a well-rounded understanding of how to approach solving process problems and how to break down a problem into its fundamental parts. In addition, it provides the science-based hypothesis testing principles that are important to understanding the solution of the problem. Chemical engineers are skilled at writing in mathematical terms the driving forces affecting processes, and are capable of modeling a process using first principles. They are able to construct a control volume for engineering balance determination across inlet and outlet streams, and use empirical methods, such as traditional regression polynomials, neural networks, or multivariate latent variable models (LVMs) to understand complex processes. The two

Chemical Engineering in the Pharmaceutical Industry: R&D to Manufacturing Edited by David J. am Ende

opposing external environment factors of setting expectations to reduce costs from consumers and the heightened scientific expectations from the regulators have created a crucial opportunity for chemical engineering principles to be applied and implemented across the industry.

In this chapter, modeling techniques applied to formulation and processing operations are discussed as support to the design, development, and scale-up for solid oral drug products. These process modeling techniques are discussed and exemplified with case studies ranging from raw material specifications to process parameter predictions. In general, the main unit operations utilized to produce tablets include blending and other powder processing, dry or wet granulation, tablet compression (powder compaction), and film coating. Specific consideration is given in this chapter to transfer and scale-up issues along with general process design related challenges to pharmaceutical process R&D.

34.1.1 Benefits of Using Modeling Tools to Design, Develop, and Optimize Drug Products

Over the last decade, pharmaceutical companies, in an effort to reduce costs, have embarked on bulk conserving methods for drug product design and development. These efforts have resulted in significant advances in process scale-up that utilize science of scale tools and predictive models. The major benefits of using modeling during development of pharmaceutical products have been previously highlighted by Wassgren and Curtis [1] who illustrated how employing reliable models can improve understanding of critical processes that may rapidly accelerate process improvements. An economic analysis of one specific engineering company utilizing computational fluid dynamics (CFD) modeling for a 6-year period revealed a sixfold return on investment (ROI) [2].

A more comprehensive economic analysis was conducted by Louie et al. [3] for the modeling of API and material science properties within the pharmaceutical development. Examples of the modeling capabilities considered in this analysis included API material properties (such as crystal morphology, surface area, and powder X-ray diffraction patterns), solubility, polymorphism, breakage planes, refractive index, molecular and solvent interactions. The benefits considered in the Louie analysis [3] included improved experimental effectiveness, broader/deeper understanding in the exploration of solution to a problem, improved productivity by employing knowledge-based reasons for moving forward, reduced time to market for new products (IP/exclusivity), and fewer unknowns with a reduced risk for failures.

The analysis indicated that the use of modeling and simulation tools in pharmaceutical development is producing an ROI of $4 to $10 per dollar invested for an occasional user to a superuser, respectively. The greatest impact on ROI was found to originate from employing superusers (or subject matter experts) in material sciences and API development. A similar analysis would be beneficial for the modeling of drug product processes during development and commercialization. The modeling capabilities available and applied to solid oral drug products consist of a balance between fundamental models, engineering-based models, and empirical models with intentional focus on applied use (Table 34.1). There

TABLE 34.1 Comparison of Modeling and Simulation Capabilities for API Material Properties Versus Solid Oral Drug Product Properties and Processes

Materials Science Modeling and Simulation of API [3]	Solid Drug Product Modeling and Simulation
Structural properties (crystal morphologies, orientations, attachment energy, surface energy, PXRD, possible API crystal forms	Raw material properties (particle size distribution, particle shape, density, material properties) [1, 4]
Physical properties (solubility, hydration, predicting preliminary physical data)	Blend properties (flow, velocity, segregation) [1, 5–10]
Molecular interactions (hydrogen bonding, solvent interactions)	Agglomeration properties (population balances of wet granulation [11])
Purity (polymorphism, impurities, predicting stability of crystal forms)	Breakage properties (population balances of milling [12])
Mechanical properties (shear strength, hardness)	Fluid dynamics (turbulent fluid flows in spray dryers, dry powder inhalers) [1]; (agitated vessels, fluidized beds) [13–15]
Thermal properties	Solid mechanics (stress analysis and density distribution for tablet and tooling) [13, 16–19]
Optical properties (refractive index, spectral absorption, circular dichroism)	Mass and energy balances (film-coating pan, fluid bed dryer) [20]
Electrical properties (conductivity, resistivity, dielectric behavior)	
Empirical models [21, 22]	Empirical models [21, 22]

appears to be a similar level of modeling and simulation capabilities for materials science of API and solid oral drug products; therefore, the authors would anticipate the return on investment for drug products to be positive also.

34.1.2 Summary of Modeling Approaches for Solid Oral Drug Products

Kremer and Hancock [13] were first to review modeling in the pharmaceutical industry and point out that process modeling can be considered as numerical simulations of the underlying physical processes. The process models in this category, which are based on first principles, can be expressed by the governing equations that are solved either analytically or numerically. The primary modeling examples presented in this chapter for the physics-based models include fluid dynamics, solids mechanics for tooling design, and particle-based models of powder discharging from hoppers.

Fluid dynamics is the study of flowing media such as gases, liquids, and certain types of solids such as dense, rapidly flowing powders. Pharmaceutical researchers have utilized commercially available CFD software packages to simulate a variety of applications including spray drying, inhalation, mixing in agitated vessels and flow of granular material. The performance of several unit operations has been investigated and optimized using CFD.

Discrete element method (DEM) is a particle-scale modeling approach in which the motion and forces associated with each particle are tracked individually. Commercial DEM software packages have only recently become available, and a specialist is often required to develop particle-based modeling using DEM. The primary disadvantage for DEM is the significant computational resources required to compute and track the wealth of particle-level information produced: particle velocities, forces, residence times, and stresses. The maximum number of particles, N, which can be modeled for reasonable simulation times is typically on the order of $N \sim 10^5$.

Engineering models can be considered a subclass of physics-based models because they are based on first principles; however, they are applied to a defined control volume typically encompassing a unit operation. These types of models are often built upon mass, momentum, and/or energy balances across the control volume, or derived from nondimensional analysis of the driving forces involved in a certain process. One example of the former (tablet film coating) and two examples of the latter approaches (wet granulation and fluid bed drying) will be discussed in this chapter. The thermodynamic film-coating model is used to scale-up the tablet film-coating process based on matching exhaust air temperature and humidity as a representation of the tablets in the coating pan (environmental similarity). Nondimensional analysis (e.g., Froude number and Reynolds number) can be employed to blending, milling and wet granulation processes to examine the specific driving forces. In addition, momentum transfer of drying air to the wet granules can be analyzed for corresponding fluidization conditions based on the granule particle size as an applied engineering approach to predict acceptable drying airflow rates.

Tablet film-coating models [20, 23–25] have been used for process scale-up based on environmental similarity in the coating pan and maintaining constant droplet size from the spray guns. The thermodynamic film-coating model has been validated across lab to production scales, and can be used to predict the temperature and relative humidity of outlet air stream, determine process set points based on desired exhaust air conditions, and minimize or eliminate the need for scale-up trials. The film-coating atomization model is a validated theoretical model that describes the film coater atomizer performance, and allows for the prediction of droplet diameter at the spray guns. The model requirements for the thermodynamic model include previous process data for the coating pan in question to generate the heat loss factor; and for the atomization model include the nozzle specifications of the spray guns and rheological properties of coating solution (viscosity, surface tension, and density).

Empirical modeling approaches are typically based on existing process data, which can yield a set of parameters that can then be interpreted from a fundamental deterministic knowledge of the process. Multivariate LVM is one specific empirical approach that has been proven to deliver a deep process understanding for unit operations that are particularly difficult to describe in a first principles model, and in situations where there is a wealth of data from the process under study [22].

The application of LVM can be better appreciated when it is mapped along the life cycle of a product/process. Although the methods can be widely applied, their application is limited by the availability of data. LVM can be applied at early stages of development, where materials (and ratios of) are being selected along with processing conditions [26]. These methods can also be applied during process design and scale-up [27] to minimize experimental work at the larger scale. For a commercial process, LVM can be used to troubleshoot/diagnosis issues [28–30], to optimize [31, 32] and to control [33–35] the operation. Other applications of LVM include the analysis of images [36, 37] and the establishment of multivariate specifications for incoming materials [38].

The first stage in the general strategy for these applications is to (i) fit a model to data, which is considered relevant to the particular application (e.g., for a monitoring application, the data will correspond to normal operating conditions, which will serve as a basis); and (ii) once the model is fitted and deemed valid, the parameters of the model are interpreted (if possible) from a fundamental perspective, trying to associate

each of the identified principal components (or latent variables) with a driving force acting upon a system.

A model that is considered valid and representative of a given system can be used in either passive mode or active mode. In passive mode, the model does not influence the process directly (e.g., troubleshooting or monitoring applications). In active mode, the model is actually influencing a decision either through a feedback control or by a design exercise.

Multivariate latent variable modeling is an alternative approach when fundamental modeling is not an option due to timing or investment constraints or lack of available fundamentals. The main difference between these types of latent variable models and other empirical approaches (such as neural networks or traditional ordinary least squares fitting) is the capabilities embedded in the method to handle massive amounts of incomplete and ill-conditioned data (which is common from an industrial process).

34.1.3 Overview of Modeling Approaches Mapped onto Unit Operations

In order to design dosage forms effectively, the engineer must be aware of the potential issues that might occur and the driving forces associated with these issues. For solid oral dosage forms produced through a dry granulation process (Figure 34.1) [39], the potential issues that can occur during process scale-up can be consider from an engineering perspective. Blending operations are intended to evenly disperse API within the excipient powder by transferring mass and energy from the mixer or impeller to the powder. Between unit operations, there often exists a transfer step that can create an opportunity for the uniform blend to segregate resulting from mass transfer. Dry granulation and milling processing is intended to reduce this segregation potential by altering the particle size distributions of active powder blend through a combination of mass and energy transfer. The goal of the tablet compression process is to produce tablets with the target product properties such as tablet weight, hardness, potency, and dissolution. This process can also be susceptible to tablet weight variations or powder segregation issues, all of which are related to the differential mass transfer, energy transfer, and momentum transfer of the materials. Film coating of tablets can exhibit issues of overdrying, overwetting, or attrition that cause defects in the final product. These issues are related to their associated driving forces of energy transfer (high drying flow rates), mass transfer (accumulation of moisture and coating from high spray rates), and momentum transfer (impacting low-density regions of tablet surfaces that attrite). The dosage form design criteria must ensure the stability, performance, and manufacturing capability of the final product. The source of the energy and/or momentum imparted onto the drug product formulation is through the processing equipment. Therefore, engineers can use energy/momentum transfer analysis as the design levers to adjust the product to the desired result in the quality attributes (e.g., blend and granulation content uniformity, tablet potency, dissolution, and stability profile).

34.2 FORMULATION MODELING

34.2.1 Empirical/Statistical Models for Raw Materials

Material properties are inherently variable, and therefore understanding the impact of these variations is an important factor in the formulation and process development of a drug product. A well designed, robust product will be minimally

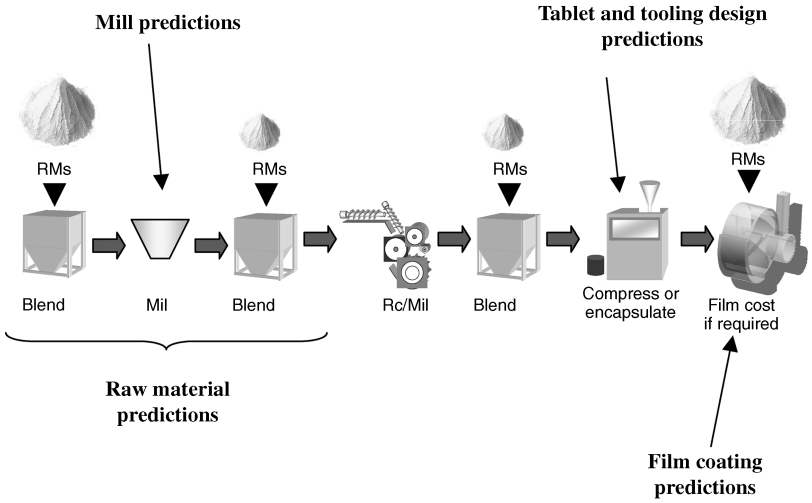

FIGURE 34.1 Modeling approaches mapped onto solid oral drug product processing [39]. Reprinted from Ref. 39 with permission of John Wiley & Sons, Inc.

sensitive to ingoing raw material changes. This section will address the relationship between the raw material variability and the drug product quality attributes, demonstrated both conceptually and through an example.

Quality should not be qualitative but quantitative, and even more, should be multidimensionally quantitative. As Duchesne and MacGregor write, "Quality is a multivariate property requiring the correct combination of all measured characteristics" [38]. So from this point and beyond, the concept of quality will not refer to a single numeric value representing a measured attribute of a product, but rather to a vector of multiple values (of multiple attributes of a product) that represent quality as a set.

Recent guidance documents from the U.S. Food and Drug Administration emphasize that quality should be built into, rather than tested on, the product [40–43]. This should be pursued from the design stages all the way to commercialization to varying degrees. Quality is defined on a case-specific basis, and in principle should be guided by the ultimate effect on product safety and efficacy and performance [44]. This guidance is referred to as the "quality by design" paradigm, and has established a science and risk based approach to pharmaceutical development and commercialization.

A process-driven design exercise is executed downstream and in sequence. Such a scenario may start with the effect of the starting material onto the first unit operation and will continue downstream with emphasis remaining on the process. It is only at the end of the process (the design of the last few unit operations of the train) that the product quality will be considered.

A quality by design exercise implies upstream design, where the design starts with a focus on the product quality and how it is impacted by the process. It continues upstream, with emphasis on the product, and ends with the analysis of the effect of the starting materials on the complete manufacturing train. This analysis will eventually end in the establishment of an acceptance criterion for each of the raw materials. These acceptance criteria will be mostly based on statistical diagnostics.

Typical statistical tools focus on testing one variable at a time in order to accept/reject a given lot of raw material. Recent trends in data analysis suggest performing this diagnosis on multiple variables simultaneously. First, a mathematical description of each of the statistical tools is required, followed by an illustration of these concepts highlighting the benefits of each technique.

34.2.2 Traditional Statistical Tools

As a well-established field, statistical diagnostics are now well accepted and widely applied in practically all areas of engineering. This section is not intended to serve as a reference in statistics; the reader is referred to other texts for this purpose [31]. What is included is a high level description of some of the concepts mentioned in statistics books so that the reader can better interpret the information presented in these.

34.2.3 A High Level View of Hypothesis Testing and Significance Levels

A set of experiments should always be carried out with a purpose in mind. The purpose is usually to obtain information from a given system and learn from it. And this learning usually comes from proving (or disproving) a preconceived idea about the system. This is referred to as hypothesis testing. The type of test used will depend on the particular hypothesis being tested, and the available data.

In engineering, hypothesis tests are usually of the quantitative nature. An inequality test—for example, is the density > 1.5 g/mL?—would require a one-sided hypothesis test, whereas a range (is the density greater than 1.5 and lower than 1.8) would require a two-sided test, and so on.

The reader should be aware that in statistics all statements involve a probability, usually referred to the level of significance, and quantified as $100(1-\alpha)$ for a given conclusion. Typical values chosen for $100(1-\alpha)$ are 95%, 99%, or 99.73% (which is the probability associated with six standard deviations or six-sigma in a normal distribution). The choice of the level of significance for a given test usually depends on the consequences and the implications (some times legal) of drawing the wrong conclusion (99% confidence on the conclusion that a plane engine will not fail means 1 in 100 times it might!). Obvious to mention is that a 95% significance level implies a value of 0.05 for α. If the test to be used is a single sided test, α is taken as is. For a double-sided test, α is usually divided by two to allow the test to be centered on the 50% probability.

Often in the establishment of specifications for materials, the hypothesis to be tested is a double-sided one. In these cases, the value of property A for a new material is compared against a reference set of values for property A to verify that it lies within a given range. The reference values for property A are usually chosen from materials used in the past due to desirability of those materials in terms of quality of the product or cost of manufacturing.

34.2.4 The Estimate of a Mean Value and Its Confidence Intervals

A simple tool to establish a double sided diagnostic to test property A for new materials is to estimate the mean value of property A and estimate the upper and lower confidence intervals for this mean value. This estimation will yield lower and upper bounds for the mean value of property A in the reference set. A new lot of raw material will be tested to determine its value of property A, and then decided if the mean

value of property A for this new lot is also a plausible (probable) mean value for property A in the reference materials.

This confidence interval is a function of the degrees of freedom (number of samples n used to estimate the mean of property A minus 1), the standard deviation of the reference values for property A and the t value from statistical tables. This t value is a function of the desired significance level (α) and a number of degrees of freedom ($n-1$). Although this t value is a strong function of α, the α value is often the less questioned parameter. For all practical purposes, α can easily be fixed (e.g., 99.73%) for the sake of testing if the mean value of a given property of a new material is the same as the one in the reference set.

Equation (34.1) describes the calculation of the confidence intervals for the mean value of a normally distributed population with unknown (only estimated) variance α^2. In practice, the factor that has the greatest impact on this calculation is the number of samples (n). The range of acceptance (upper minus lower bound) will be large for a small number of samples, and will asymptotically narrow as the number of samples increases.

$$\bar{x} - t_{\alpha/2,n-1}\sigma/\sqrt{n} \leq \mu \leq \bar{x} + t_{\alpha/2,n-1}\sigma/\sqrt{n} \qquad (34.1)$$

In this formula, σ is the calculated standard deviation, $\bar{x}$ is the calculated average, n is the number of samples considered, and $t_{\alpha/2,n-1}$ refers to the value of t for a significance level of $100(1-\alpha)$ and $n-1$ degrees of freedom; this value is taken from statistical tables.

For example, consider three sample sets taken from the same population. All sample sets with an average of 4.25, and standard deviations of 0.0470, 0.0565, and 0.0895, respectively, which were calculated using 30, 10, and 3 samples. At a 95% level of significance the values of t for $n = 30$, 10 and 3 are 2.042, 2.26, and 4.3, respectively. With these values, the confidence intervals on the means for each population are given in Table 34.2. Notice the dramatic increase in the range, just due to the number of samples considered in the calculations. The data for this example are from a pharmaceutical grade polymeric material and are a real illustration of how acceptance limits can vary in an application. The practitioner is encouraged to sample properly to avoid artificially large acceptance regions simply due to a limited number of samples available.

TABLE 34.2 Confidence Intervals for the Mean Value of Three Sample Sets of the Same Population

Mean Value	Sample Sets of Same Population		
	$n = 30$	$n = 10$	$n = 3$
Mean lower bound	4.234	4.214	4.027
Mean upper bound	4.268	4.295	4.472
Range	0.03397	0.08088	0.44471
% Change from $n = 30$	0	138.12	1209.27

34.2.4.1 Emerging Multivariate Techniques A natural implication of the evolution of analytical technology is the fact that a given material can be characterized by a large number of attributes. It is the duty of the engineer to determine which of these attributes are relevant to the product/process. The answer to this question for a pharmaceutical product is rarely a single property (a scalar), and more often a set of properties (a vector) that will impact the product or process. The challenge now is how to establish a specification for multiple quantities.

The simple solution to this challenge is to establish multiple univariate diagnostics using traditional statistical tools described previously. This practice, however, implies that all the measured characteristics for the new material can be tested and assessed independently of each other. This assumption falls apart quite easily for complex materials where a large number of properties are related. For example, for a polymeric material the molecular weight distributions (or compositional distributions for a copolymer) are not independent of viscosity or density, which can also be linked to cross-linking.

In such a situation, there is a need for a tool that will enable the establishment of acceptance criteria for multiple properties simultaneously, accounting for their correlated nature. It is no longer enough to know the desired level (mean) and tolerance for each property. Additional information is necessary to account for the dependencies across the multiple properties being tested.

Multivariate LVMs have been proposed in literature to address this need. LVMs will empower the user to establish diagnostics and acceptance criteria based on a model of the data [38].

34.2.4.2 Using a Model to Establish a Test of Acceptance Before describing the calculations behind a multivariate specification, it is important to discuss the overall strategy of using a model (any model!) to establish acceptance regions. To illustrate this point, consider the case of a material that is characterized by two properties A and B (plotted in Figure 34.2 where each dot is plotting the numerical values of property A versus property B for a given lot of raw material). Assume also that there is enough data to conclude that the lots of material represented by gray markers are desirable, and those represented by black dots correspond to undesirable material.

The challenge is to somehow delineate the region spanned by the gray markers. If univariate measures are taken (define a lower and upper bound for property A and B separately) one would end with a region equivalent to the smallest square that fits in the "gray marker" zone (drawn with a dotted line square). Although feasible and simple, this may constrain the practitioner to a very small region of acceptance and will end in large amounts of rejected material.

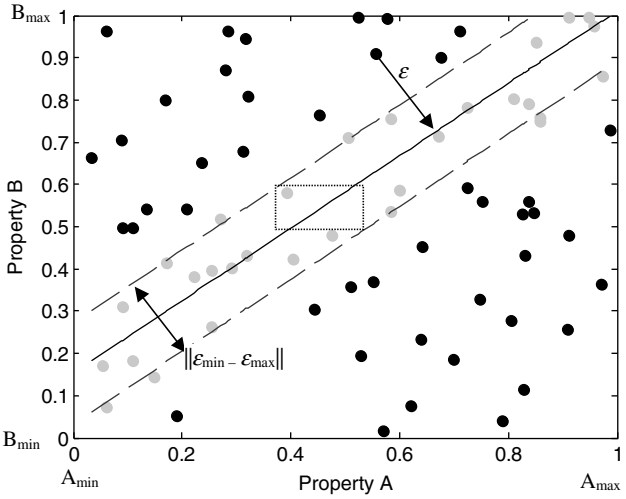

FIGURE 34.2 Conceptual illustration of a case where a multivariate specification is required.

The alternative is to use mathematics to delineate this region. Taking all the data that correspond to the gray markers, a regression model can be fitted. The regression line given by $A_{gray} = mB_{gray} + \delta$ is illustrated with a black line in Figure 34.2 (where m and δ are fitted parameters from the data).

This simple model (a line) can then be used to quantify the perpendicular distance from any given point, to the regression line (illustrated as ε in Figure 34.2).

The set of distances (ε) for all the gray points can be used to determine a maximum and minimum ε (ε_{min} and ε_{max}). These limits (ε_{min} and ε_{max}) on the perpendicular distance and the regression model and the upper–lower boundaries (A_{min}, A_{max}, B_{min}, and B_{max}) can be used to establish a multivariate specification that will ensure properties A and B for a new lot are within the region spanned by the gray markers. There is still a delicate statistical exercise, that is, to determine the perpendicular distance to tolerate (given by $||\varepsilon_{min} - \varepsilon_{max}||$), this will determine the width of the acceptance region (region bounded by the dashed lines in Figure 34.2) and the risk associated with the test.

For this conceptual case, the steps to accept a new lot of material (with properties A and B equal to a_{new} and b_{new}, respectively) using the overall bounds, a simple regression line as a model and an acceptable perpendicular distance (ε) would be as follows:

(i) If $A_{min} < a_{new} < A_{max}$ and $B_{min} < b_{new} < B_{max}$ continue, otherwise reject a_{new} and b_{new}.

(ii) Calculate $\varepsilon = a_{new} - (mb_{new} + \delta)$.

(iii) If $\varepsilon_{min} \leq \varepsilon \leq \varepsilon_{max}$, then the new lot is not rejected (there is no statistical evidence to prove that this lot of material is any different from the population represented by the gray markers in Figure 34.2).

Step (i) will ensure that the values of a_{new} and b_{new} are at least within range, step (ii) uses the model to determine the perpendicular distance to the line that runs in the middle of the acceptance region, step (iii) determines if this perpendicular distance is within tolerance. Notice that the model is *not* being used for predictive purposes.

Both properties (A and B) still need to be measured and none of them are being predicted from the other. The model in this case is just a mere geometrical tool to delineate a region that is one degree of complexity beyond a simple squared region (which is the result of two univariate specifications together). Also notice that there is still an exercise of probability and risk analysis associated with determining the upper and lower bounds for the key diagnostic(s) involved (in this case ε_{min} and ε_{max}). The strategy proposed here is multivariate in the sense that it handles more than one variable, but more important, it is multivariate simultaneous, which means it handles more than two properties at the same time.

For the conceptual case illustrated in Figure 34.2, it is easy to see how a line can be used as a model in the specification since the data are composed of two properties. As the dimensionality of the problem increases (the amount of variables to consider simultaneously) so does the need to have a model that considers all variables, their uncertainty levels and correlation simultaneously. And for that, principal component analysis is suggested.

34.2.4.3 Principal Components Analysis Principal component analysis (PCA) is a well-established technique to project or compress data to a lower number of new variables called principal components. Geometrically, the PCA works by identifying a new coordinate system within the data (see Figure 34.3), so that each point can be referred to by its coordinates with respect to this new system. Hopefully, the number of coordinates needed to span data well enough will be dramatically less than the original number of variables. The example in Figure 34.3 illustrates a data set with three variables (X_1, X_2, and X_3) that can significantly be represented with a two-dimensional coordinate system, assuming the deviation from this plane (see Figure 34.3b) is negligible.

Many software packages[1] are available in the market to fit a PCA model, and therefore such calculation is not discussed here. A PCA model is quite powerful as a tool to establish specifications due to the diagnostics provided by the model. This application is extensively discussed in literature [4, 38] and only summarized in this chapter.

Once a PCA model is fitted, each of the observations used in the model can be summarized by two overall diagnostics, the squared prediction error (SPE) and the Hotelling's T^2 statistic.

[1] www.umetrics.com; www.prosensus.ca; www.camo.com; www.eigenvector.com

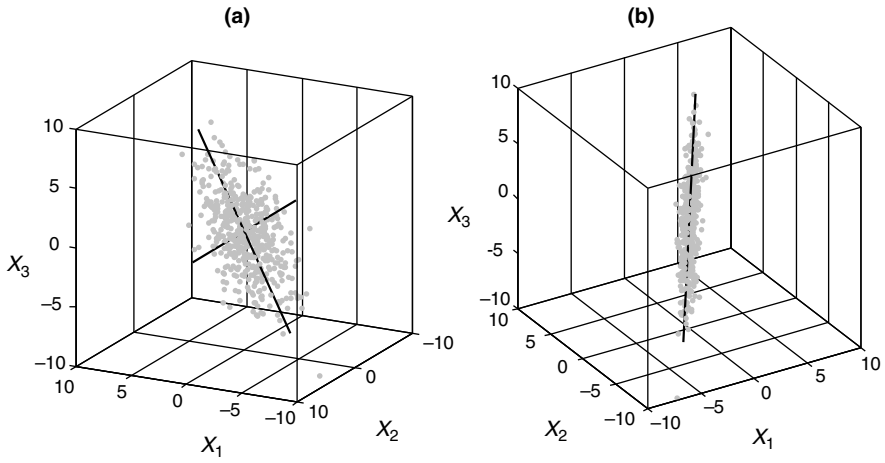

FIGURE 34.3 Dimension reduction of a 3D data set to a 2D plane by PCA.

34.2.4.4 The Squared Prediction Error This diagnostic is identical in interpretation to the perpendicular distance (ε) mentioned in the conceptual problem presented previously in this section. This is a quantitative measure on how well the new sample adheres to the structure of the reference data. This is a positive number and is well accepted to follow a chi-squared distribution [45], which means that confidence intervals for a given level of significance can be computed.

34.2.4.5 The Hotelling's T^2 Statistic This diagnostic is a measure of the squared distance from the origin of the data (the mean values) to the expected conditional value for the properties of the new lot. In the conceptual problem, this would be equivalent to the square of the distance along the black line (illustrated with an arrow), from the center of the box to the intersection where b_{new} meets $\hat{a}$, which is given by the regression model (Figure 34.4). Since the model prediction is being used here, it is imperative to first assess that the SPE is within tolerance. Notice that imposing a bound on this diagnostic, implicitly imposes a bound on the magnitude of properties A and B, and hence, step (i) in the suggested sequence, could be replaced by a simple one-sided test on the Hotelling's T^2 diagnostic.

The use of these multivariate diagnostics is illustrated with an example taken from a real scenario in the pharmaceutical sector.

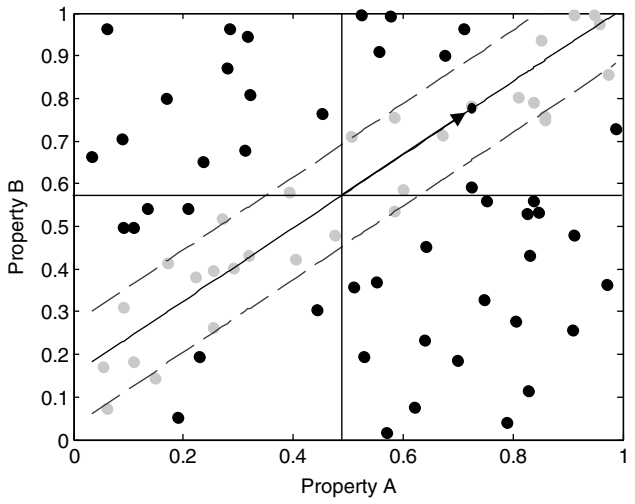

FIGURE 34.4 Conceptual problem illustrating the distance being diagnosed by the Hotelling's T^2 in a two-dimensional problem.

EXAMPLE 34.1 SETTING MULTIVARIATE RAW MATERIAL SPECIFICATIONS USING PCA

Consider a polymeric ingredient that is characterized by three descriptors of its particle size: D_{10}, D_{50}, and D_{90} (each number represents the average size at the tenth, fiftieth, and ninetieth quantile from the distribution). Each quantity is reported in logarithmic scale in Table 34.3. This table also contains the lower and upper limits for the mean, as calculated from this table. The fundamental concept to illustrate is that these three descriptors for particle size are not independent of each other, and a change in one of them will imply a change in the others (Figure 34.5).

Consider now six new lots of material (data provided in Table 34.4). If the three independent specifications are used to decide weather to accept or not these six lots of material, it is quite obvious that the lots 1, 5, and 6 (marked by a ●, ▼, and ★, respectively) will be rejected. In contrast, a principal component analysis model was fitted to the data using one significant component, the Hotelling's T^2 and the SPE diagnostic, and finally a multivariate specification was built (Figure 34.6 where the new lots are colored in gray). Notice that this specification also rejects lots 1, 5, and 6, however, lots 3 and 4 (marked by ▲ and ♢, respectively) are rejected and only lot 2 (marked by a ■) is accepted. The reason is

TABLE 34.3 Example of Data from a Polymeric Pharmaceutical Excipient Used in Example 34.1

Sample	$\log_{10}(D_{10})$	$\log_{10}(D_{50})$	$\log_{10}(D_{90})$
Lot 1	4.17	4.57	5.42
Lot 2	4.17	4.59	5.48
Lot 3	4.19	4.57	5.43
Lot 4	4.19	4.57	5.37
Lot 5	4.20	4.53	5.40
Lot 6	4.20	4.54	5.37
Lot 7	4.22	4.58	5.40
Lot 8	4.22	4.58	5.40
Lot 9	4.22	4.59	5.39
Lot 10	4.23	4.60	5.44
Lot 11	4.23	4.60	5.40
Lot 12	4.23	4.59	5.44
Lot 13	4.23	4.57	5.44
Lot 14	4.23	4.59	5.40
Lot 15	4.24	4.60	5.41
Lot 16	4.25	4.59	5.38
Lot 17	4.25	4.61	5.40
Lot 18	4.25	4.62	5.46
Lot 19	4.25	4.61	5.44
Lot 20	4.26	4.58	5.46
Lot 21	4.26	4.59	5.45
Lot 22	4.27	4.58	5.43
Lot 23	4.27	4.62	5.44
Lot 24	4.28	4.62	5.41
Lot 25	4.29	4.61	5.47
Lot 26	4.31	4.67	5.51
Lot 27	4.31	4.64	5.46
Lot 28	4.31	4.65	5.47
Lot 29	4.32	4.63	5.47
Lot 30	4.32	4.63	5.49
Lot 31	4.32	4.63	5.52
Lot 32	4.35	4.67	5.50
Mean	4.25	4.60	5.44
Standard deviation	0.047	0.032	0.041
n	32.00	32.00	32.00
$t(\alpha/2),n$ [$\alpha = 0.05$]	2.042	2.042	2.042
Mean low limit	4.23	4.59	5.42
Mean upper limit	4.27	4.61	5.45

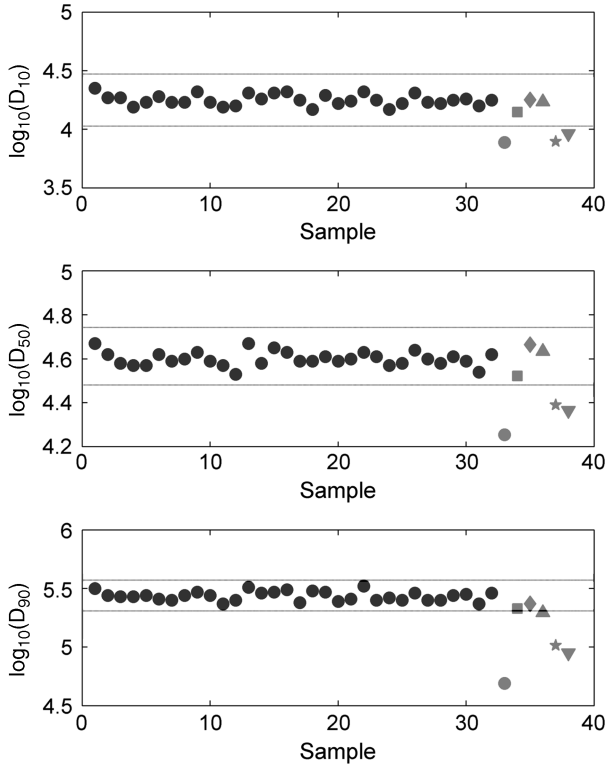

FIGURE 34.5 Univariate specifications and acceptance criteria for particle size descriptors. Black markers denote reference lots and gray markers denote new lots to be tested for acceptance.

TABLE 34.4 Data for Six New Lots of Polymer for Example 34.1

New lot	$\log_{10}(D_{10})$	$\log_{10}(D_{50})$	$\log_{10}(D_{90})$
A	3.9	4.2	4.7
B	4.1	4.5	5.3
C	4.2	4.7	5.4
D	4.2	4.6	5.3
E	3.9	4.4	5.0
F	4.0	4.4	4.9

simple to understand by looking at the three descriptors simultaneously, as shown in Figure 34.7.

In the top plot of Figure 34.7, lots 1, 5, and 6 were rejected because all three particle size descriptors are clearly different from the lots used as a reference. The bottom plot (which is a rotated version of the top) illustrates why lot 2 (marked by a ■) was accepted while lots 3 and 4 (marked by ▲ and ♢) were rejected. The particle size descriptors for lot 2 exhibit the same expected proportions between the $\log_{10}(D_{10})$, the $\log_{10}(D_{50})$, and the $\log_{10}(D_{90})$ (referred to as covariance structure) as in the reference set and hence it is safer to accept this material than other materials where the proportions between these properties is different. An added advantage of the multivariate specification (Figure 34.6) is that a single plot can be used to impose specifications on multiple properties simultaneously. For this case, it was possible to visualize the three particle size variables in a three dimensional plot; a real case scenario may consist of several hundreds of variables, and then the power of a multivariate approach is the ability to still monitor the multivariate proportion of the all properties, simultaneously in a couple of plots.

Ultimately, the impact of the raw material physical and chemical properties on the final drug product depends on the manufacturing process (e.g., wet granulation will be affected by properties that don't affect dry granulation). This section exemplified a general method to establish specifications on

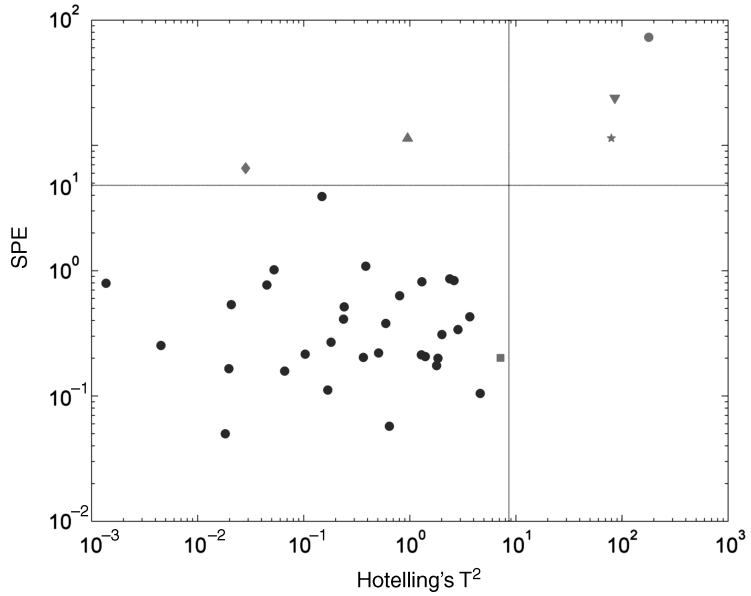

FIGURE 34.6 Multivariate specification for particle size data in Example 34.1 with acceptance limits. Black markers denote reference lots, gray markers denote new lots to be tested for acceptance.

the properties of a given material. The Section 34.3 focuses on unit-operation specific details where the relevance of certain physical/chemical properties of the material are discussed in the context of the processing route.

34.3 PROCESS MODELING FOR SOLID ORAL DRUG PRODUCT PROCESSES

34.3.1 Powder Flow Models

34.3.1.1 Model Development for Powder Processes Using Discrete Element Method The DEM is one possible approach to model powder flow in processing operations. DEM models are a computational approach whereby the state of each particle in the system is tracked at each instant in time. These models produce a wealth of particle-level data including particle positions and velocities as well as the forces acting on each particle. These data can then be used to calculate many other useful quantities such as velocity profiles, stress tensors, solid fractions, and local mass fractions. This wealth of data is a key advantage of the DEM approach; many of these quantities are expensive and difficult, if not impossible, to measure experimentally. However, acquiring these data via DEM does have significant costs, primarily in long computational times. Depending on the number of particles modeled, the complexity of the simulation domain, and the length of time modeled, simulation times may range from a few hours to well over a month of computing time. Thus, high-speed computers and efficient software algorithms are quite important to obtain results in reasonable times.

The algorithm of a typical DEM model is shown in Figure 34.8. The simulation is initiated by defining the computational domain and creating particles within it. Each particle is given a size, mass, and density and assigned a position and velocity. The simulation is started and all contacting pairs (both particle–particle and particle–wall) are identified. This step is among the most time consuming aspect of DEM programs. A brute force algorithm that searches between all possible pairs scales with N^2, where N is the number of particles in the simulation. However, using techniques such as a neighbor searching algorithm can reduce the time to the order of N Ln (N). Once each contacting pair is identified, force–displacement models are used to determine the contact forces acting on each of the particles. While several such models can be used, most models specify the normal and tangential forces as a function of the overlap distance between particles (the overlap approximates particle deformation during contact and is typically constrained to a small value ($<$1% of particle diameter)). For example, one such model for the normal force is based on the theoretical work by Hertz [46] in 1882. This model describes the elastic contact of a sphere, and gives the normal force, $\mathbf{F}_N$, as

$$\mathbf{F}_N = k_N \delta^{3/2} \hat{\mathbf{n}} \tag{34.2}$$

where k_N is a stiffness related to the radii and material properties of the contacting spheres, δ is the overlap distance between the spheres and $\hat{\mathbf{n}}$ is the unit normal vector. Other, more complex, models build upon this and other theories to include dissipative effects for modeling inelastic contacts. In

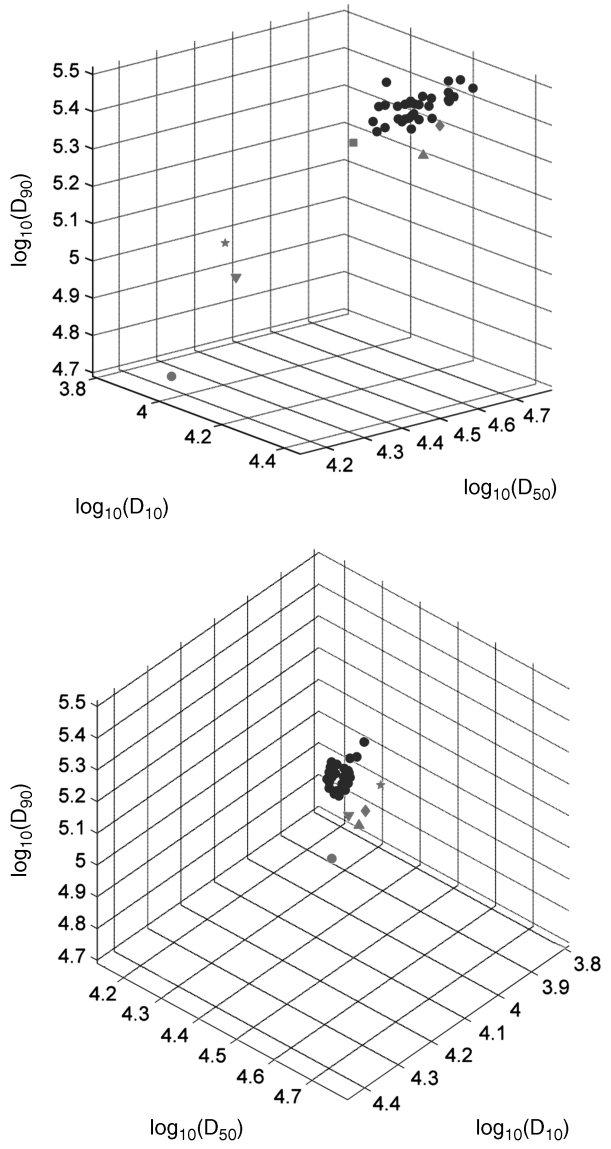

FIGURE 34.7 Three particle size descriptors plotted simultaneously black markers denote reference lots, gray markers denote new lots to be tested for acceptance. Bottom plot is a rotation of the top plot.

addition to the normal and tangential contact forces, body forces—such as the acceleration due to gravity, electrostatics, and magnetic fields – can also be included. The resultant contact and body forces acting on each particle are summed. Newton's second law is then used to calculate the translational and rotational accelerations, respectively:

$$\mathbf{F}_{N,\text{Total}} = m\frac{\partial^2 \mathbf{x}}{\partial t^2} \tag{34.3}$$

$$\mathbf{M}_{\text{Total}} = I\frac{\partial^2 \theta}{\partial t^2} \tag{34.4}$$

where $\mathbf{F}_{N,\text{Total}}$ is the total, resultant normal force acting on a given particle, m is the particle mass, $\mathbf{x}$ is the particle position vector, t is time, $\mathbf{M}_{\text{Total}}$ is the total, resulting moment due to the tangential forces acting on a given particle, I is the particle moment of inertia, and θ is the particle orientation vector. Subsequently, these accelerations are integrated in time to determine updated particle velocities and positions. At this point, virtually any quantity of interest may be measured and the simulation then proceeds to the next iteration by incrementing the time step and repeating the necessary contact detection calculations. This procedure is repeated until the simulation has reached the desired end point, such as when a hopper is completely discharged.

Often times, certain assumptions are made in DEM models to simplify the computational demands. For example, assumptions of spherical particles, cohesionless particles, and negligible interstitial fluid effects are often made. Each of these assumptions help to not only make the simulations faster but also make the modeled system less representative of the real system of interest. Ongoing research efforts currently are working toward relaxing these assumptions from the models, and many recent research papers describe work where one or more of these assumptions have been removed. Interested readers are referred to review papers [6, 47, 48] and the references therein for more detailed information.

34.3.1.2 Powder Discharge and Segregation Modeling Using DEM The drug product manufacturing process typically involves several powder handling operations that are used to create the final product—a dosage form such as a tablet or capsule—from several raw materials—typically powders with varying physical and chemical properties. In all cases, content uniformity is a critical quality attribute of the final dosage form. The drug loading in each dosage form is important because if this were to vary considerably, patients would receive doses that might be ineffective or possibly result in undesired side effects or worse. Detailed guidelines issued by the United States Pharmacopeia (USP) state the acceptance limits of variability in drug loading and prescribe the testing procedure used to determine the variability of a particular batch [49].

There are many powder processing unit operations used in the manufacture of tablets and capsules. These operations include blending, hopper filling and discharge, and flow through various feeding or dispensing devices, to name but a few. The object of the blending process is, as the name suggests, to combine the raw material powders into a well-mixed blend containing a uniform distribution of all materials. This is not a trivial task, as each raw material consists of particles with a range of sizes and morphologies. Differences in these properties will cause particles to segregate or de-mix. If this occurs in a blender, it may be difficult or impossible to achieve a well-mixed blend. Assuming that a uniform

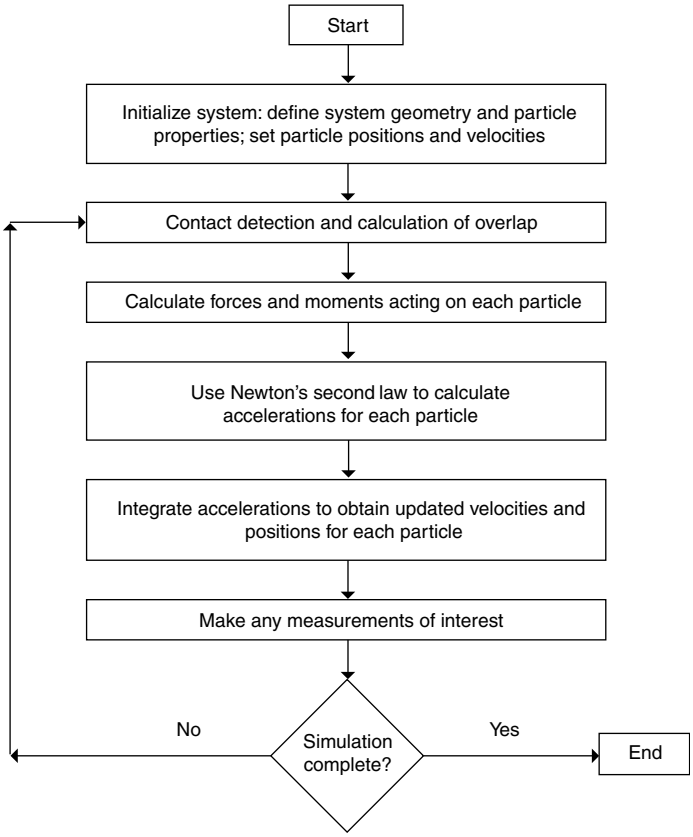

FIGURE 34.8 A flowchart showing the algorithm typically used in Discrete Element Method simulations of powder flow [6]. Reprinted from Ref. 6 with permission of John Wiley & Sons, Inc.

mixture can be obtained in a blender, segregation in subsequent operations can lead to content uniformity that is out of specification. It should be noted here that blend uniformity is not the sole concern of a formulation scientist. Other properties such as flowability and compressibility may present similar constraints on the development and processing of a drug product formulation. Nevertheless, in the remainder of this section, we will focus on content uniformity.

Hopper filling and discharge is one common operation that occurs downstream from blending operations. Therefore, it is critical that the hoppers are filled in a manner that does not cause the uniform blend to segregate. Additionally, it is important that the hopper design and raw materials—to the extent that their properties can be modified or selected—be designed to minimize segregation during the hopper discharge process. If these hopper flows and other subsequent operations such as flow through a tablet press feeder do not induce segregation of the blend, favorable content uniformity results should be obtained.

Here, we show an example of how the DEM as described earlier can be used to computationally model powder flow and gain a better understanding of the powder dynamics. While DEM models can be useful for discerning a wide variety of data from powder flows, we will focus on segregation of a binary mixture. This example will show how the DEM approach can be used to determine the effect of particle size ratio on the extent of segregation during hopper discharge. Consider a binary mixture of spherical particles—one species with a large diameter and the second species with a smaller diameter. While typical pharmaceutical formulations contain several different components, we presently assume a binary mixture where the small species represents the API and the larger species represents all of the excipients (diluents, binders, disintegrants, lubricants, etc.). Typically, the API particle size is much smaller than most of the excipients, and the ratio of these size differences can affect the degree of segregation during hopper discharge.

The model hopper is filled with the binary mixture containing 5% by mass of the smaller species. The initial state is well mixed, which permits analysis of the segregation during the discharge event only. A similar model could be developed to model the combined filling and discharge processes. Figure 34.9 shows an image taken from the simulation after the hopper is filled and discharge has been initiated. This model uses periodic boundaries to enable modeling just a thin slice of a larger hopper with a rectangular cross section.

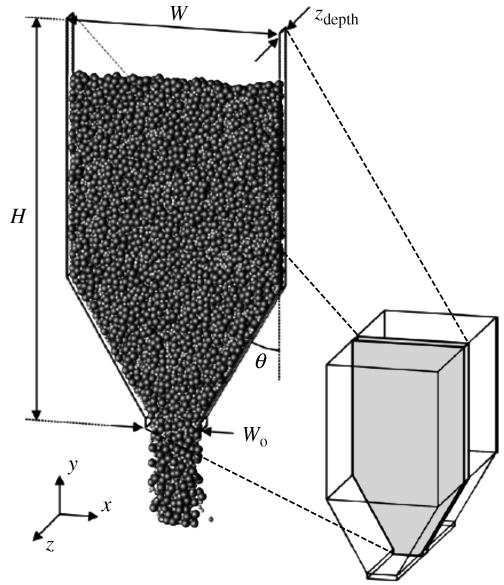

FIGURE 34.9 A simulation image showing a DEM model of hopper discharge [8]. Reprinted from Ref. 8 with permission of John Wiley & Sons, Inc.

As the mixture is discharged, the simulation program tracks the time at which each particle is discharged. These data are analyzed and the fines mass fraction is calculated. Figure 34.10 shows the plots of the normalized fines mass fraction, x_i/x_f, where x_i is the fines mass fraction of a given sample of the discharge stream and x_f is the fines mass fraction of the initial blend charged to the hopper as a function of the fractional mass discharged M/M_{Total} where M is the cumulative mass discharged and M_{Total} is the mass of material initial charged to the hopper. For all size ratios, the discharge stream is relatively well-mixed for the first 30% of the discharge process. Then, for the cases with larger particle diameter ratios, Φ_D, a depletion in the smaller species is observed. This is followed by a spike in the fines mass fractions near the end of hopper discharge ($M/M_{Total} > 80\%$). These results show that discharge of a well-mixed pharmaceutical blend from a hopper may result in significant content uniformity issues if the particle size ratio is greater than ~2. For $\Phi_D = 6.7$, tablets produced during the middle of the batch may only have ~50% of the expected API, while tablets produced at the end of the batch could have over 200% of the expected API.

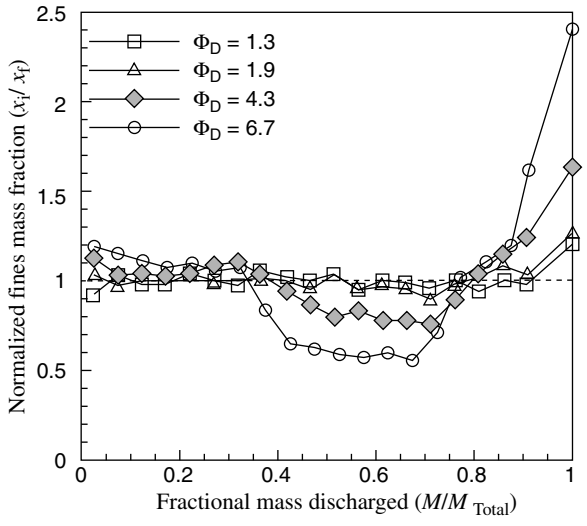

FIGURE 34.10 Segregation of a binary mixture of the given particle size ratios during discharge from a hopper [8]. Reprinted from Ref. 8 with permission of John Wiley & Sons, Inc.

The simulation animations also provide insight into the flow dynamics that might be difficult to observe experimentally. In fact, in such an animation, one can observe the small particles segregating via the sifting or percolation mechanism [50]. During this process, small particles preferentially move in the direction of gravitational acceleration through a matrix of larger particles. This process causes an accumulation of fine particles near the hopper walls that gets discharged last. The material from which the fines sifted can now considered to be depleted in fines. This fines-depleted material generally exits the hopper after 40% of discharge but less than 70% of discharge according to Figure 34.10.

In practice, these potency variations within a batch can occur. However, they typically do not reach these extremes. Due to several assumptions in this example model, most predominantly that of cohesionless particles, the model predicts the worst case scenario in terms of segregation potential. The inclusion of cohesive forces in the model would tend to reduce the extent of segregation as the particles, once in a well-mixed state, will have reduced freedom to move relative to one another and segregate. Nevertheless, the model described here with cohesionless particles helps to improve process understanding and guide process development and scale-up decisions.

This example has illustrated how the DEM approach can be used to gauge the segregation potential during hopper discharge for a range of particle size ratios. The effects of other particle properties—such as density, shape, and surface roughness—and hopper geometries—such as the hopper wall angle, diameter, outlet diameter, and wall roughness can also be modeled using the same approach [8]. Similarly, other processes such as blending and hopper filling can also be modeled with DEM.

In this section, we have reviewed the importance of maintaining content uniformity during hopper discharge and highlighted one of the methods by which segregation of materials can be modeled. In the next section, we discuss modeling of wet granulation, a process that helps to bind particles of different materials together, thereby reducing the potential for segregation in subsequent processing and handling operations and improving the likelihood of good content uniformity in the final dosage form.

34.3.2 Wet Granulation Process Models

34.3.2.1 Model Development for Wet Granulation Using Engineering Principles Wet granulation is a particle size enlargement process that is commonly used in the manufacture of drug product dosage forms. There are several reasons to wet granulate pharmaceutical blends. Increasing the particle size will tend to improve flow. Fine powders usually have significant cohesive forces between the constituent particles that act to retard flow. By enlarging the particle size, these cohesive forces become less significant compared with the particle mass, thereby improving the flowability of the bulk powder. Another reason to granulate includes reducing the potential for segregation of the API. The wet granulation process physically binds the blended particles together thereby reducing the likelihood that one species will segregate and cause potential content uniformity problems.

Wet granulation processes are often carried out as batch processes using high-shear mixers as shown in Figure 34.11. While wet granulation can also be conducted in other equipment such as planetary mixers, fluidized beds, or extruders, high-shear mixers are the most common in the pharmaceutical industry and will be our focus in this section. In the high-shear mixer, a centrally located impeller (in this case, a top-driven impeller is shown although some high-shear mixers utilize a bottom-driven impeller) is used to mix and consolidate the granulation. A chopper (located on the left side of this schematic) spins at a high speed and helps to break up very large granules. Finally, a spray nozzle (not shown in Figure 34.11) is used to add a liquid granulating agent. This liquid may contain a liquid binder or may consist only of water when a dry binder has already been added to the formulation.

Granulation in a high-shear mixer begins with the addition of the dry powder blend and dry mixing with the impeller for a short period of time. With both the impeller and the chopper rotating, the liquid addition phase begins. After the desired amount of liquid has been added, the "wet massing" phase begins where the impeller and chopper continue to mix the granulation while the liquid addition is stopped. In general, the point at which to stop the granulation process (the process end point) is difficult to determine scientifically and is still a matter of ongoing research. In the past, skilled operators would deem a granulation complete if it passed the so-called *squeeze test* where a small amount of material is squeezed in one's hand and subjectively observed. Many different researchers have proposed various ways to monitor the high-shear wet granulation process in a more objective manner. Some of these approaches include impeller power or torque, off-line measurement in a torque rheometer, as well as some more recent analytical techniques such as using near-infrared (NIR) and focused beam reflectance measurement (FBRM). Several of these techniques are discussed further in a recent review [51].

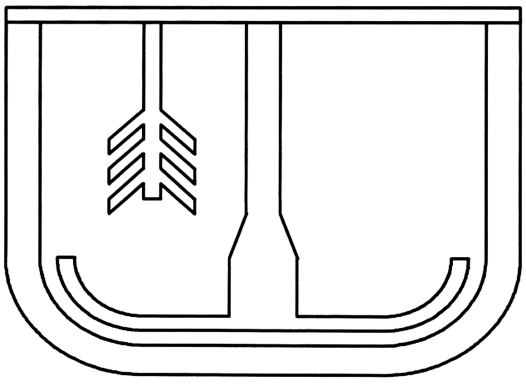

FIGURE 34.11 A schematic of a high shear wet granulator [57]. Reprinted from Ref. 57, Copyright (1999), with permission from Elsevier.

A second area of difficulty with high-shear wet granulation processes revolves around process scale-up. Many of the process parameters such as impeller speed, water addition amount, water addition rate, and wet massing time are determined through experimental design of experiments (DOEs). However, the process dynamics change significantly as larger scale granulators are used. Hence, similar DOEs are conducted at each of the scales during the process scale-up effort. These experiments consume significant labor resources and also incur large raw material costs if granulations of proprietary APIs in limited quantities are being conducted. This is especially true at the largest of scales where batch sizes may be on the order of 1000 L. Thus, the use of models to (1) predict process parameters for scaling-up and (2) determine when to stop the wet granulation process (end point) can be extremely useful.

34.3.2.2 Wet Granulation Scale-Up Process scale-up in pharmaceutical industry is driven by two important factors: (1) cost of API, which usually runs into several thousand dollars per kilogram of material, and (2) tight product specifications as desired by various stages of clinical trials. The practical considerations demand that in a pharmaceutical industrial setting, a wet granulation process can be developed that is cost-effective, robust, and deliver products with high quality. The process development and scale-up from lab scale to pilot scale or commercial scale broadly takes place in two steps that are described below [52].

Formulation Development and Optimization The process and formulations are developed and optimized in a small granulator, typically at one L lab scale using few hundred grams of API, through detailed experimentation. The main goal of this experimentation is to explore the design space of the process parameters such as the total amount of binder and its rate of addition, impeller speed, total processing time, dry powder fill height, and end point. This exploration should result in a process that yields granules with desired size and

porosity distribution, which can be compressed into tablets with the desired quality attributes including hardness–compression behavior and dissolution profiles.

Process Development and Scale-Up After the design space is explored and the formulation is optimized at lab scale, it is scaled up to pilot or production scale. Essentially, a process template is developed at lab scale and it has to be replicated at a much larger scale that results in product with similar quality attributes. Several routes to process scale-up have been demonstrated by various groups, mostly applicable to a specific set of granulators and limited formulations [51]. Almost all the procedures of scale-up are based on the similarity between the two granulators of interest. Formally, the similarity principal for a process is established using dimensional analysis. The application of the similarity principal begins with the recognition that any physical process can be represented by a dimensional relationship between n process variables and constants as shown below.

$$F(X_0, X_1, X_2, \ldots, X_n) = 0 \tag{34.5}$$

The above relation can be reduced by applying Buckingham Π theorem, which simply states between $m = n - r$ mutually independent dimensionless groups, where r is the number of dimensional units, that is, fundamental units (rank of the dimensional matrix). The equation (34.5) can be reduced to the following relationship.

$$F(\Pi_0, \Pi_1, \ldots, \Pi_n) = 0 \tag{34.6}$$

The above relationship can be rewritten by expressing first dimensionless group in terms of the rest of them as shown below.

$$\Pi_0 = f(\Pi_1, \Pi_2, \ldots, \Pi_n) \tag{34.7}$$

It must be noted that the similarity analysis should be applied to processes where a clear understanding of process is established.

Scale-Up Approach 1

The earliest application of similarity analysis for the scale up of wet granulation process was demonstrated by Leunberger and coworkers at University of Basel and Sandoz AG [53–56]. The physical relationship used to describe the granulation process can be written as

$$P = f(\rho, D, \Omega, q, t_p, V_b, H, g) \tag{34.8}$$

The description of various physical quantities is shown in Table 34.5.

The above relationship is nondimensionalized using d, $1/\omega$, and ρd^3, as length, time, and mass scales, respectively. The dimensionless quantities are shown in Table 34.6.

These investigators performed wet granulation experiments using a placebo formulation (86% w/w lactose, 10% w/w corn starch, and 4% w/w polyvinylpyrrolidone as binder) in mixers of planetary type (e.g., Dominici, Glen, and Molteni). The batch size ranged from 3.75 up to 60 kg. The impeller speed was scaled using a constant Froude number ($d_1\omega_1^2 = d_2\omega_2^2$). The volume fraction and geometric ratio were also kept constant. It was seen that the power profile measured during the granulation can be divided into five different phases (S_1–S_5) as shown in Figure 34.12. It was found that the amount of binder liquid added during the process varies linearly with the batch as shown in Figure 34.13. Therefore, the functional relationship between dimensionless groups is as follows:

$$\Pi_0 = f(\Pi_1) \tag{34.9}$$

From these findings, one can conclude that the correct amount of granulating liquid per amount of particles to be granulated is a scale-up variable. It is necessary, however, to mention that during this scale-up exercise only a low-viscous granulating liquid was used. The exact behavior of a granulation process using high-viscous binders and different batch sizes is unknown. It is shown that the first

TABLE 34.5 List of Important Process Variables and Parameters That Define a Wet Granulation Process in Scale-Up Approach 1

No.	Quantity	Symbol	Units	Dimension
1	Power consumption	P	Watt	ML^2T^{-3}
2	Specific density	ρ	kg/m^3	ML^{-3}
3	Impeller diameter	D	m	L
4	Revolution speed	Ω	rev/s	T^{-1}
5	Binder flow rate	q	kg/s	MT^{-1}
6	Bowl volume	V_b	m^3	L^3
7	Gravitational constant	g	m/s^2	LT^{-2}
8	Bowl height	H	m	L
9	Process time	t_p	s	T

TABLE 34.6 Dimensionless Numbers and Groups Used in Scale-Up Approach 1

Number	Symbol	Dimensionless Group	Description
1	Π_0	$P/(d^5\omega^3\rho)$	Power number
2	Π_1	$qt_p/V_b\rho$	Specific amount of liquid binder
3	Π_2	V/d^3	Volume fraction of dry powder
4	Π_3	$(d\,\omega^2)/g$	Froude number (centrifugal force/gravitational force)
5	Π_4	H/d	Geometric ratio

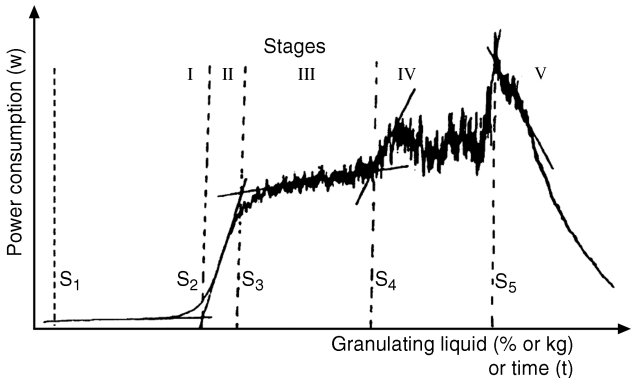

FIGURE 34.12 Division of a power consumption curve [55]. Reprinted from Ref. 55, Copyright (2001), with permission from Elsevier.

derivative of the power consumption curve is a scale-up invariant and it is proposed that it can be used as an in-process control or a fine-tuning of the correct amount of granulating liquid.

Scale-Up Approach 2

One of the key assumptions made in this study that the viscosity of the wet mass is unimportant, may not hold true for many formulations and viscous binders. Rowe and coworkers [57, 58] developed a different approach to scale up wet granulation process. These authors defined the process by following relationship.

$$\Delta P = f(\rho, R, \Omega, \mu, R_b, g, m) \qquad (34.10)$$

The description of the various physical quantities is shown in Table 34.7. The above relationship can be nondimensionalized using d, $1/\omega$, and ρd^3, as length, time, and mass scales, respectively. The dimensionless quantities are shown in Table 34.8.The power number is expressed as a function of the other dimensionless quantities as follows:

$$\log_{10}(N_P) = a \cdot \log_{10}(\psi Re \cdot Fr \cdot \text{fill ratio}) + b \qquad (34.11)$$

where a and b are regression constants. Faure et al. [57] carried out wet granulation experiments of lactose and maize starch-based placebo formulations in a series of Collette Gral Granulators with sizes 8, 25, 75, and 600 L. They fitted the experimental data with equation 34.11 and found that the regression coefficient was $r^2 > 0.88$ using the data from the 8, 25, and 75 L bowls with PTFE lining, and the 600 L bowl that did not require the lining (see Figure 34.14). The slope was found to be $a = -0.926$, and the intercept $b = 3.758$. This work shows that a nonlinear scale-up relationship exists between wet granulation carried out in geometrically similar granulators of different sizes. Moreover, this relationship can be effectively used when scaling up the process from one size to another size. In the next section, a case study is presented, which demonstrates the application of above-mentioned scale-up approaches.

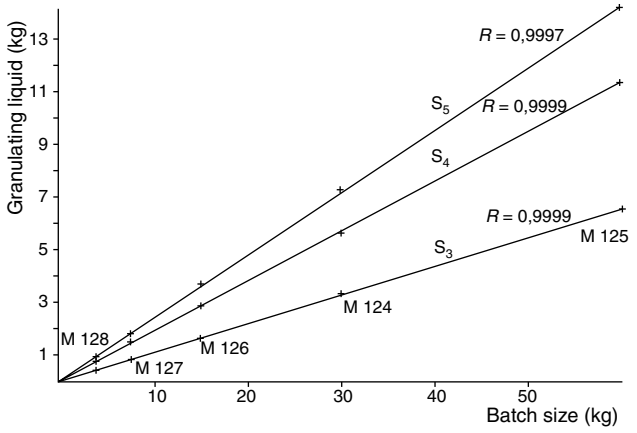

FIGURE 34.13 Scale-up precision measurements with identical charges [55]. Reprinted from Ref. 55, Copyright (2001), with permission from Elsevier.

TABLE 34.7 List of Important Process Variables and Parameters That Define a Wet Granulation Process in Scale-Up Approach 2

No.	Quantity	Symbol	Units	Dimension
1	Net power consumption	ΔP	Watt	ML^2T^{-3}
2	Wet mass density	ρ	kg/m^3	ML^{-3}
3	Impeller radius	R	m	L
4	Revolution speed	Ω	rev/s	T^{-1}
5	Wet mass consistency/ viscosity	μ	Nm	ML^2T^{-2}
6	Bowl radius	R_b	m	L
7	Gravitational constant	G	m/s^2	LT^{-2}
8	Amount of wet mass	M	kg	M

TABLE 34.8 Dimensionless Numbers and Groups Used in Scale-Up Approach 2

No.	Symbol	Dimensionless Group	Description
1	N_P	$\Delta P/(d^5\omega^3\rho)$	Power number
2	ψRe	$\rho R^2\omega/\mu$	Pseudo Reynolds number (inertial force/viscous force)
3	Fr	$(R\omega^2)/g$	Froude number (centrifugal force/gravitational force)
4	Fill ratio	$\rho R_b^3/m$	Fill ratio (granulator volume/wet mass)

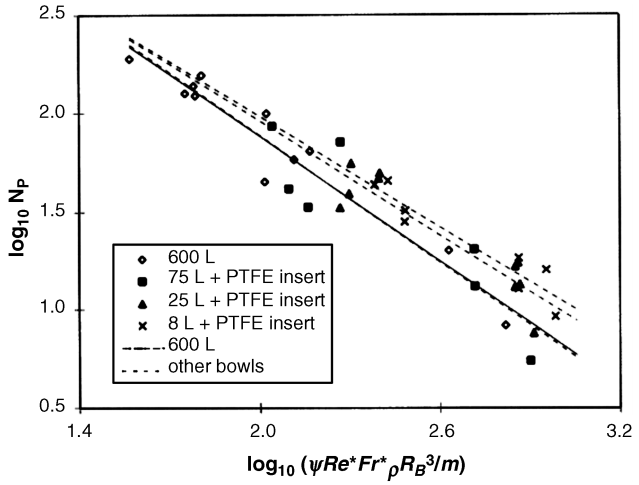

FIGURE 34.14 Dimensionless power relationship of the 600 l Collette Gral mixer-granulator [57]. Reprinted from Ref. 57, Copyright (1999), with permission from Elsevier.

EXAMPLE 34.2 SCALE-UP OF WET GRANULATION USING ENGINEERING MODELS

A wet granulation process is carried out for a placebo formulation with water as a binding liquid, in an 8 L Collette Gral granulator. The process parameters are optimized for desirable end point through a design of experiments study. These parameters are listed in Table 34.9. This process is to be scaled-up to a granulator with 75 L capacity such that the final product is of the same quality. In this, case the product quality is identified by the specific density and wet mass consistency of granules at the end point. Hence, desirable end point is one that gives product with essentially the same specific density and wet mass consistency or viscosity obtained at 8 L scale. There are three main process parameters that are to be determined at 75 L scale, (a) impeller rotation speed, (b) amount of water used, and (c) power consumption near the end point. All these quantities will be calculated using above discussed scale-up approaches.

Solution

(a) The impeller rpm is scaled using constant impeller tip speed:

$$\Omega_2 = \Omega_1\left(\frac{r_1}{r_2}\right)$$
$$\Omega_2 = 350\left(\frac{0.12}{0.25}\right) = 164\,\text{rpm} \qquad (34.12)$$

(b) The amount of water used at 75 L scale is determined by assuming water to dry powder weight ratio is invariant across the scales.

TABLE 34.9 Process Variables and Parameters for Two Different Collete-Gral Bowl Sizes Used in the Example 34.2

Process Parameters and Variables	Units	8 L Bowl	75 L Bowl
Impeller radius	m	0.119	0.254
Bowl radius	m	0.123	0.262
Revolution speed	1/s	5.83	2.73
Revolution speed	1/min	350.0	**164.0**
Dry powder weight	kg	1.50	14.00
Total water added	kg	0.50	**4.67**
Gravitational constant	N/m^2	9.81	9.81
Bulk density	kg/m^3	400.0	400.0
Viscosity	N/m	0.30	0.30
Power consumption	Watt	127.7	**3503**
Froud number		0.41	0.19
Pseudo Reynolds number		110.1	235.1
Fill ratio		0.37	0.38
Power number		67.41	405.8
$\log(N_P)$		1.83	2.61
$\log(Re^*Fr^*\text{fill ratio})$		1.23	1.24
Scale-up constant a		−0.93	−0.93
Scale-up constant b		3.76	3.76

Bolded values are calculated by scale-up rules.

$$\text{Water used at 75 L} = \frac{(\text{amount of water used at 8 L}) \times (\text{dry powder mass at 75 L})}{(\text{dry powder mass at 8 L})}$$
$$\text{Water used at 75 L} = \frac{(0.5\,\text{Kg}) * (14\,\text{Kg})}{(1.5\,\text{Kg})} = 4.67\,\text{Kg} \qquad (34.13)$$

(c) Finally, the power consumption at the end point is determined using scaling relationship given by equation 34.11 as follows:

$$\begin{aligned} Fr &= 0.19 \\ \psi Re &= 235.1 \\ \text{Fill ratio} &= 0.38 \\ \log_{10}(N_P) &= -0.926 * \log_{10}(0.19 * 235.1 * 0.38) \\ &\quad + 3.758 \\ N_P &= 405.8 \\ \Delta P &= N_P * (\rho\Omega^3 R^5) = 3503\,\text{W} \end{aligned} \qquad (34.14)$$

The process parameters for both the scales are listed in Table 34.9. The power calculated using the above scale-up approach is used to guide determination of the wet granulation end point. However, it must be kept in mind that this scale-up approach, like any other approach based on dimensional analysis, is semiempirical in nature and needs some experimental work to achieve optimum scale-up and process

design. This approach should be contrasted from a process model based on fundamental principles, which requires material properties and process parameters to achieve optimum design.

34.3.2.3 Fluidization Regime During Granule Drying In the area of fluid bed drying of granules produced by wet granulation processing, there is an engineering approach to assess fluidization regimes *a priori* if the particle size distributions and equipment airflows are known. A semiempirical approach in that empirical heat transfer data is required for the simulations to compare favorably with experiment, has been used to predict process parameters for fluidization properties in a fluid bed dryer. Based on the mean diameter of the granule distribution, the process map shows the proposed equipment is adequate to fluidize the granules in the desired bubbling regime (Figure 34.15). Granule characteristics, such as moisture content and granule size distribution, are known for a particular product entering the fluid bed dryer. The range of volumetric flow rates of the drying gas and the dimensions of the air inlet were obtained from the equipment manufacturer. Finally, a review of the literature indicated that researchers had constructed models to predict both the minimum fluidization velocity and the transitions to turbulent and fast fluidization.

The granules produced through wet granulation and dried through fluid bed drying are finally compressed into tablets (Figure 34.1). The focus of this section was on the use of modeling to achieve consistent granulation properties on scale-up to assure consistent input to the tableting process. Tableting is an important unit operation for solid dosage manufacturing since it defines the dosage strength and performance. In the next section, some of these models employed to understand compaction of blends into tablet will be discussed in detail.

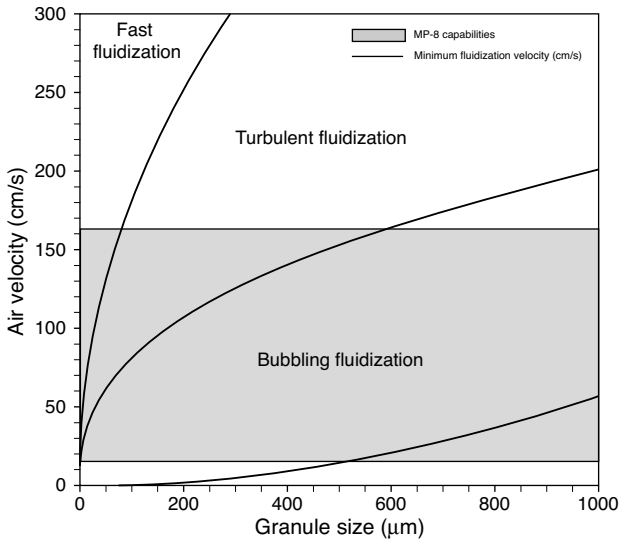

FIGURE 34.15 Engineering model of granule fluidization using empirical relationships found in literature based on granule distribution and equipment airflow [14, 15]. (Courtesy of D.M. Kremer.)

34.3.3 Tablet Compression Models

34.3.3.1 Principles of Finite Element Analysis A finite element analysis/method (FEA/FEM) is a numerical approach to solve a partial differential equation. It is widely used in engineering and science as many physical phenomena can be described in terms of a partial differential equation. The technique consists of the following steps:

1. Subdividing the problem domain (or geometry) into finite elements connected together by nodes. These finite elements are commonly termed as a *mesh*.
2. Development of equations (such as force and mass balance) for each element and then assembling them for the entire domain or system of elements.
3. Solving the resulting system of equations.
4. Analyzing quantities of interest such as stresses and strains and obtain visualizations of the response of the system to the applied loadings.

Powder Compaction Tablet compression is an important unit operation in the pharmaceutical industry as it significantly affects the mechanical strength and relative density of the drug product. Finite element analyses are a common method that is employed to study the tableting process where the formulation powder is assumed to be a continuum material [59–62]. The approach is based on the following components:

- Continuity equations (e.g., conservation of mass)
- Equilibrium equations (e.g., force balance on the material)
- Initial and boundary conditions of the problem
- Dynamics of the loading and the geometry of the problem
- Constitutive behavior of the powder (e.g., stress–strain relationships)

Due to the availability of powerful, inexpensive computers and commercial finite element software, the continuity and equilibrium equations can be solved accurately and quickly after the appropriate boundary conditions are defined. Moreover, it is possible to define a complex sequence of loading and unloading steps such as the compression, decompression and ejection during model setup. However, it is a challenge to obtain model inputs to the FEA solver [60–64] such as the constitutive relationships of the formulation

powder (e.g., stress–strain relationships) and friction between powder and die wall to get accurate estimation of the powder stress levels during tableting. The following section highlights some of the commonly used constitutive relationships for the powder continuum.

34.3.3.2 Tablet Finite Element Analysis

Powder Material Models The stress–strain relationships for powders were originally developed for classical soil mechanics applications and were used to simulate compaction of ceramic powders. They were assumed to be elastic-plastic materials and appropriate relationships were developed to describe the yield surface of the material. There are a number of phenomenological models to describe the yield surface of the powder materials such as the Gurson model [16], Cam Clay model [17] and the Drucker–Prager cap plasticity (DPC) model [18, 19]. The DPC model has been widely used [59, 62, 64–67] in comparison with the other models for two main reasons: firstly, it can efficiently capture the shear failure during the decompression and ejection phase of the tableting process and secondly, because experiments on real powders can be designed to efficiently characterize its parameters. The stress–strain relationship and the yield loci used in the DPC model are shown in Figure 34.16. The yield surface consists of three segments: a shear failure surface, a "cap" surface that represents plastic compaction or inelastic hardening and a transition surface between them. The transition surface is introduced for smooth numerical implementation. For a detailed description of the equations of the different yield surfaces of the DPC model and the experimental procedure to obtain its parameters, refer to Han et al. [60] or Cuningham et al. [59].

Applications FEA analyses performed using the DPC material model has been used to study the elastic recovery or "springback" of material during the compression and ejection phases of tableting that leads to capping incidence in tablets [64, 67]. The relative density distribution after ejection [62, 66] and temperature distribution in the compact and tooling during compaction [68] have also been investigated using FEA methods. Moreover, the stresses during the different tableting stages (see Figure 34.17) have been analyzed and correlated to possible tablet failure mechanics [60, 67].

This section summarized the concept of applying a continuum based finite element model to predict the stresses on a tablet during tableting operations. Further investigation is necessary to establish if these predicted stresses and density distributions by FEA have an implication in understanding possible failures that might occur in other unit operations, such as during tablet film coating. The next section explains the tablet-coating operation and available engineering models used to predict the coating process parameters.

34.3.4 Tablet Film-Coating Models

34.3.4.1 Model Development for Film Coating Using First Law of Thermodynamics Tablet film coating is a widely used unit operation within the pharmaceutical industry for applying both aesthetic and functional coatings on tablets. Color coating is often used in combination with tablet shape to enable manufacturers, pharmacists, and patients to distinguish between not only different products but also different dosage strengths within the same product. From a physical standpoint, a thin film-coat layer can improve the mechanical integrity of the tablets and also make them smoother, which improves tablet flowability, enhances packaging efficiency, and increases palatability for patients. Film coating can improve functionality by providing a barrier against environmental exposure to moisture, light, or air. This can enhance product stability and reduce the requirement for more expensive packaging materials. In some cases, the color

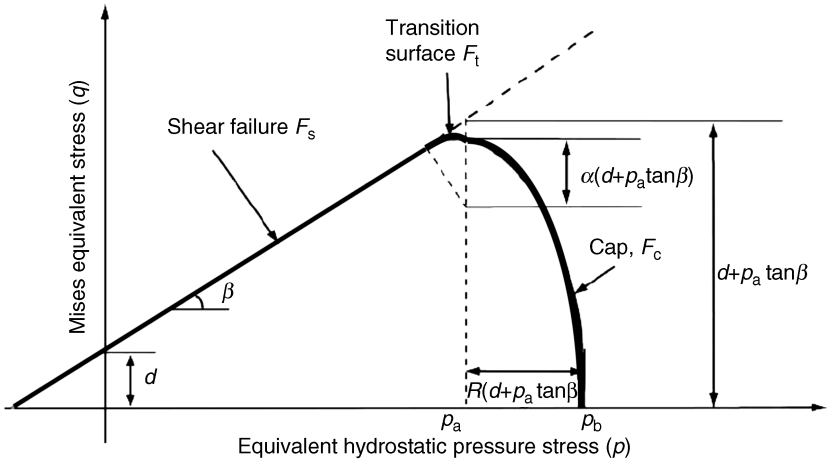

FIGURE 34.16 Drucker–Prager cap model. Yield surface in the pq-plane [60]. Reprinted from Ref. 60, Copyright (2008), with permission from Elsevier.

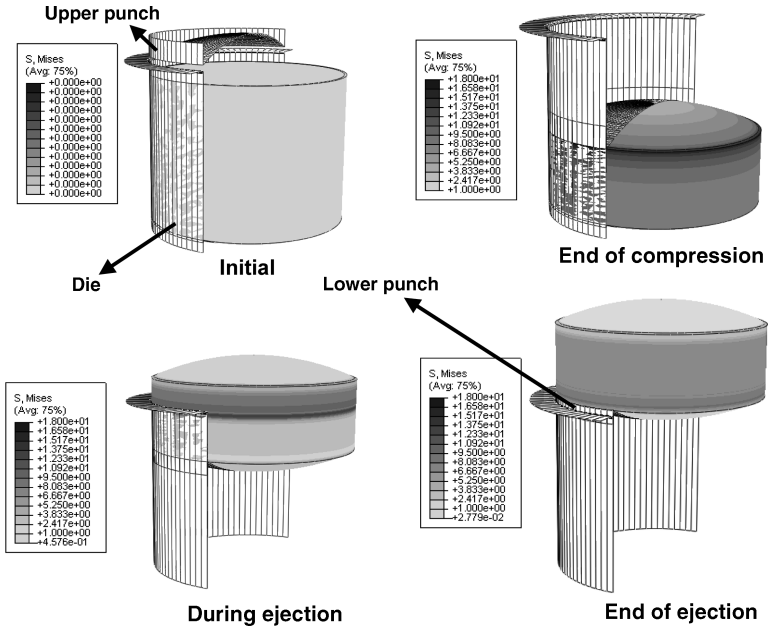

FIGURE 34.17 Stress distributions on the tablet during compaction using a standard round concave (SRC) punch.

of a tablet can be an important part of brand recognition and can even be used to trademark.

Typically coating formulations can be either aqueous or solvent-based systems. While aqueous coatings are rapidly becoming the preferred method for many applications, solvent-based coatings are still used to apply many functional coatings onto tablet cores for controlled drug delivery (e.g., semipermeable or delayed/sustained-release membranes) [69]. Although solvent-based systems hold a number of advantages in terms of application and flexibility, the move to aqueous coatings has largely been driven by factors such as cost, safety concerns, more stringent regulations on effluent discharge, as well as the broad variety of film formulations that have been developed recently for aqueous application [70].

The film coating process can essentially be considered an adiabatic evaporative cooling process. The driving energy for fluid evaporation is a combination of the airflow volume, temperature, and moisture content of the air. This can be considered as the bulk gas phase in total. The underlying law controlling the thermodynamic environment within the process is the first law of thermodynamics (conservation of energy). It is important to understand that the three principles of driving energy are linked by the operating parameters within the process. For example, an increase in the inlet air temperature will lower the relative humidity of the drying air into the pan (although the absolute water content remains the same). Increasing the spray rate of the coating solution will increase the moisture content of the air in the pan to which the tablets are exposed. Once stabilized, however, the process will remain in equilibrium unless disturbed by the alteration of a process parameter or external condition. Since the quality of the overall coating is greatly influenced by the thermodynamic conditions inside the pan, it is of great importance to understand these relationships and how to control them.

Thermodynamic models utilizing material and energy balances have been used in the past with some success to model the aqueous film coating process [23–25, 70, 71]. These models are used to predict the key process parameters that impact the quality of the film coat; mainly exhaust air temperature and exhaust air relative humidity. Film-coating models are particularly important in pharmaceutical development where process conditions vary greatly for the purpose of design of experiment, scale-up, and coating formulation changes. Most of the previous models have been restricted to aqueous film coatings, and one coating pan type or scale, making them limited in their scope and applicability. More recently, am Ende and Berchielli developed a universal thermodynamic model that is applicable to both aqueous and organic film-coating systems to aid in process optimization and scale-up [20]. This model will be the basis for the discussion and calculations laid out in the following section. Whether the system in question is aqueous or organic based, the film-coating process is a delicate balance that requires a high level of control over the process conditions to produce films that provide the required aesthetics or functionality.

34.3.4.2 Model System, Assumptions, and Limitations

A typical tablet film coater schematic is shown in Figure 34.18 for a perforated coating pan. The drying air is heated by an external heating source to a target temperature,

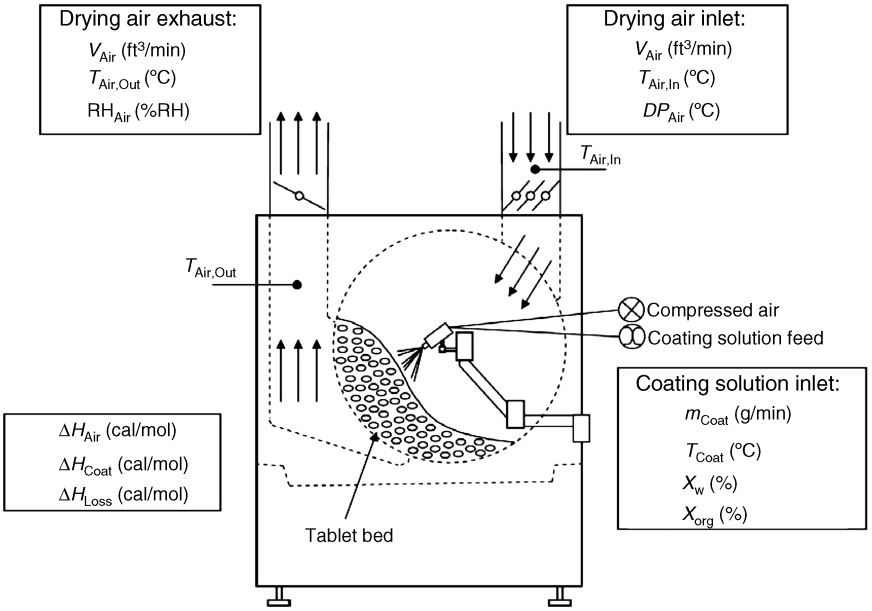

FIGURE 34.18 Schematic of a typical perforated tablet film-coating pan.

$T_{air,in}$, which is typically controlled by the operator to target a desired exhaust air temperature, $T_{air,out}$. The air flows through the tablet bed where it serves to dry the damp tablets as the coating solution droplets impact and spread on the tablet face. The air exits the pan through the exhaust air duct at a lower temperature due to the evaporative cooling effect from the volatile components (aqueous or organic) in the coating solution. The coating solution is supplied to the spray nozzle(s) by a pump where it is atomized by a compressed air stream into a pattern of tiny droplets that are propelled from the nozzle toward the tablet bed.

The rotating tablet bed defines the control volume for the material and energy balances. The model applies to steady-state conditions where the heat, temperature and mass do not change with time:

$$\frac{dq}{dt} = \frac{dT}{dt} = \frac{dm}{dt} = 0 \tag{34.15}$$

The inlet streams to the system include the drying air, and the film-coating solution. The compressed air stream is neglected in the overall airflow through the pan since it is only a minor component compared to the drying air. The outlet stream consists of the drying air exhaust and it is assumed that the volatile components in the coating solution exit the coater through this stream as vapor (i.e., the tablets do not retain any moisture). This is a reasonable assumption since coating pans are typically overdesigned with regards to drying capacity. The model was developed for a closed but not isolated system since energy exchange occurs as heat loss from the pan during operation and sampling. The model also neglects the humidity from the compressed air as well as the sensible heat term for the solid components of the coating solution.

This film-coating model is a macroscopic analysis of the process and, therefore, the physical operating conditions such as the spray gun-to-bed distance, pan speed, pan load, and spray zone coverage are not considered. It is well known that these parameters also influence key tablet attributes such as coating uniformity and elegance, and, therefore, they should be monitored carefully during process optimization.

34.3.4.3 Material Balance The material balance for the tablet bed control volume can be expressed in terms of each of the three components involved (e.g., water, organic solvent, and air). Assuming no reaction or accumulation the total mass entering the system should be equal to the total mass exiting the system:

$$\sum m_{in} + \sum m_{coat} = \sum m_{out} \tag{34.16}$$

The material balance for water takes into account the humidity from the inlet drying air stream as well as the water in the coating solution:

$$m_{w,in} + m_{w,coat} = m_{w,out} \tag{34.17}$$

where $m_{w,in}$ is the mass flow rate of water in the inlet air stream, $m_{w,coat}$ is the mass flow rate of water in the coating solution, and $m_{w,out}$ is the mass flow rate of water in the outlet air stream.

For coating formulations with organic components, the material balance can be expressed as

$$m_{org,coat} = m_{org,out} \tag{34.18}$$

where $m_{org,coat}$ is the mass flow rate of organic in the coating solution and $m_{org,out}$ is the mass flow rate of organic in the outlet air stream.

Neglecting the contribution from the compressed air line to the spray nozzle the material balance for air can be expressed as follows:

$$m_{\text{air,in}} = m_{\text{air,out}} = V_{\text{air,in}}\,\text{ft}^3/\text{min} \times \left(\frac{28.3\,\text{L/ft}^3 \times 29\,\text{g/mol}}{22.4\,\text{L/mol}}\right) \times \left(\frac{273\,\text{K}}{273\,\text{K} + T_{\text{air,in}}}\right) \tag{34.19}$$

where $m_{\text{air,in}}$ is the mass flow rate of air in the inlet air stream, $m_{\text{air,out}}$ is the mass flow rate of air in the outlet air stream, and $V_{\text{air,in}}$ is the volumetric flow rate of air in the inlet air stream.

This equation converts the volumetric flow rate of the inlet air stream to a mass flow rate and incorporates a correction to account for change in molar volume of air due to the elevated temperature, $T_{\text{air,in}}$, at the inlet flow meter.

34.3.4.4 Energy Balance The overall energy balance for the system can be expressed based on the first law of thermodynamics as follows:

$$\Delta H = \Delta H_{\text{air}} + \Delta H_{\text{coat}} + \Delta H_{\text{loss}} = 0 \tag{34.20}$$

where ΔH is the overall enthalpy change across the control volume and individual terms, ΔH_{air}, ΔH_{coat}, and ΔH_{loss}, represent the enthalpy change across the control volume due to the drying airflow, the coating solution, and heat loss, respectively. The individual enthalpy terms can be expressed in terms of a sensible heat term and, where applicable, a latent heat of vaporization.

$$\Delta H = mC_{\text{p}}\Delta T + m\Delta\hat{H}_{\text{vap}} \tag{34.21}$$

The enthalpy change for the airflow then becomes

$$\Delta H_{\text{air}} = m_{\text{air,in}}C_{\text{p,air}}\left(T_{\text{air,out}} - T_{\text{air,in}}\right) \tag{34.22}$$

where $C_{\text{p,air}}$ is the heat capacity of air, $T_{\text{air,out}}$ is the temperature of the exhaust air, and $T_{\text{air,in}}$ is the temperature of the inlet air.

Since the tablet bed temperature, T_{tablet}, typically is not measured during normal operation it is assumed to be the same or similar as the exhaust air temperature. Therefore, the sensible heat term in the coating solution enthalpy change is defined in terms of the temperature difference between the exhaust air and the coating solution temperature, T_{coat}. Thus, the enthalpy change for the coating solution can be written as

$$\Delta H_{\text{coat}} = m_{\text{w,coat}}C_{\text{p,w}}\left(T_{\text{air,out}} - T_{\text{coat}}\right) + m_{\text{w,coat}}\Delta\hat{H}_{\text{vap,w}} + m_{\text{org,coat}}C_{\text{p,org}}\left(T_{\text{air,out}} - T_{\text{coat}}\right) + m_{\text{org,coat}}\Delta\hat{H}_{\text{vap,org}} \tag{34.23}$$

$$m_{\text{w,coat}} = x_{\text{w}}m_{\text{coat}} \tag{34.24}$$

$$m_{\text{org,coat}} = x_{\text{org}}m_{\text{coat}} \tag{34.25}$$

where $C_{\text{p,w}}$ is the heat capacity of water, $C_{\text{p,org}}$ is the heat capacity of the organic component, $\Delta\hat{H}_{\text{vap,w}}$ is the latent heat of vaporization for water, $\Delta\hat{H}_{\text{vap,org}}$ is the latent heat of vaporization for the organic component, T_{coat} is the temperature of the coating solution (assumed to be room temperature), x_{w} is the mass fraction of water in the coating solution, x_{org} is the mass fraction of organic in the coating solution, and m_{coat} is the mass flow rate of the coating solution.

The enthalpy change for the heat loss to the surroundings can be expressed as

$$\Delta H_{\text{loss}} = h_{\text{loss}}A\left(T_{\text{air,out}} - T_{\text{RT}}\right) \tag{34.26}$$

where h_{loss} is the heat transfer coefficient, A is the surface area for heat loss, and T_{RT} is the room temperature.

Since the heat transfer coefficient and surface area for heat loss can differ greatly between coating pans, these two terms are lumped together into an empirically determined heat loss factor (HLF):

$$\Delta H_{\text{loss}} = \text{HLF}\left(T_{\text{air,out}} - T_{\text{RT}}\right) \tag{34.27}$$

The overall energy balance can be obtained by substituting the individual enthalpy terms into equation (34.20) as follows:

$$\Delta H = m_{\text{air,in}}C_{\text{p,air}}\left(T_{\text{air,out}} - T_{\text{air,in}}\right) + x_{\text{w}}m_{\text{coat}}C_{\text{p,w}}\left(T_{\text{air,out}} - T_{\text{coat}}\right) + x_{\text{w}}m_{\text{coat}}\Delta\hat{H}_{\text{vap,w}} + x_{\text{org}}m_{\text{coat}}C_{\text{p,org}}\left(T_{\text{air,out}} - T_{\text{coat}}\right) + x_{\text{org}}m_{\text{coat}}\Delta\hat{H}_{\text{vap,org}} + \text{HLF}\left(T_{\text{air,out}} - T_{\text{RT}}\right) = 0 \tag{34.28}$$

The energy balance equation can then be rearranged to solve for the unknown exhaust air temperature:

$$T_{\text{air,out}} = \frac{m_{\text{air,in}}C_{\text{p,air}}T_{\text{air,in}} + x_{\text{w}}m_{\text{coat}}C_{\text{p,w}}T_{\text{coat}} - x_{\text{w}}m_{\text{coat}}\Delta\hat{H}_{\text{vap,w}} + x_{\text{org}}m_{\text{coat}}C_{\text{p,org}}T_{\text{coat}} - x_{\text{org}}m_{\text{coat}}\Delta\hat{H}_{\text{vap,org}} + \text{HLF} \times T_{\text{RT}}}{m_{\text{air,in}}C_{\text{p,air}} + x_{\text{w}}m_{\text{coat}}C_{\text{p,w}} + x_{\text{org}}m_{\text{coat}}C_{\text{p,org}} + \text{HLF}} \tag{34.29}$$

The thermodynamic film-coating model detailed above provides a direct relationship between inlet air temperature, drying airflow rate, coating solution spray rate, and composition to the temperature of the exhaust air stream. Once the HLF is determined for a specific coating pan, the model can be used to predict the exhaust air temperature based on the operating conditions of the coater. The percent relative humidity of the exhaust air stream ($\%\text{RH}_{\text{out}}$) can be calculated based on the material balance for water around the control volume and then taking the ratio of the partial

pressure of water vapor in the exhaust air ($P_{w,out}$) to the vapor pressure of water at the exhaust air temperature ($P^*_{w,Tair,out}$):

$$\%RH_{out} = \frac{P_{w,out}}{P^*_w(@T_{air,out})} \times 100\% \quad (34.30)$$

34.3.4.5 Prediction of Target Film-Coating Parameters Using Thermodynamic Model Before the predictive capabilities of the thermodynamic film-coating model can be utilized a value for the HLF must be determined for the specific coating pan in question. The model outlined in equation (34.29) has two unknowns, the HLF and the exhaust air temperature, $T_{air,out}$. The HLF can be determined empirically by comparing equation (34.29) to a set of experimental data where the exhaust air temperature has been measured. The HLF is used as a variable fitting parameter to minimize residual sum of squared error between the experimental data and the predicted exhaust air temperature from the model. This can be done with any simple optimization function such as Solver in Microsoft Excel®. A sample data set with an optimized heat loss factor calculation for a Vector HCT-30 model film coater is shown in Table 34.10. The data include both aqueous and organic coating formulations for a wide range of operating conditions (inlet temperature, airflow, and spray rate). By minimizing the sum of squared error between the actual and the predicted exhaust air temperature the HLF was determined to be 150 cal/min°C.

Once the HLF is determined the model can be used for process optimization and scale-up predictions for that specific pan. For example, an operator can see how a change in spray rate or drying airflow will affect the exhaust air temperature of the process. The operator can also determine what inlet air temperature set point will be required to target a specific exhaust air temperature in the coater.

EXAMPLE 34.3 THERMODYNAMIC FILM-COATING MODEL

A small-scale Vector LDCS-5 film coater has a HLF of 282 cal/min°C. (a) Determine the required inlet air temperature set point to achieve a target an exhaust air temperature of 50°C at an airflow of 40 ft^3/min, and a spray rate of 4 g/min. The coating solution is an aqueous formulation with 20 wt% solids and the room temperature is 22°C. The heat capacity of air and water, and the latent heat of vaporization of water can be readily found in any physical chemistry textbook. (b) What is the relative humidity of the exhaust air at these conditions if the dew point of the inlet air is 10°C?

Solution

(a) Equation (34.29) cannot easily be rearranged to solve for the inlet air temperature, $T_{air,in}$, since this term is embedded in the denominator of equation (34.19) to calculate the mass flow rate of air in the coater. Therefore, the equation must be solved iteratively by guessing a value of $T_{air,in}$ and solving for $T_{air,out}$. Since we know $T_{air,in}$ must be higher than $T_{air,out}$ a good initial guess might be 20°C higher than the target exhaust temperature (i.e., $T_{air,in} = 70°C$). Thus, from equation (34.19)

$$m_{air,in} = 40\,ft^3/min \times \left(\frac{28.3\,L/ft^3 \times 29\,g/mol}{22.4\,L/mol}\right) \times \left(\frac{273\,K}{(273 + 70°C)K}\right) = 1166.45\,g/min$$

TABLE 34.10 Sample Data Set with Heat Loss Factor Determination for an HCT-30 Film Coater

Trial	Acetone (%)	Water (%)	Room Temperature (°C)	Inlet Temperature (°C)	Drying Airflow (ft^3/min)	Spray Rate (g/min)	Actual $T_{air,out}$ (°C)	Predicted $T_{air,out}$ (°C)	Difference Predicted - Actual
1	85	5	22	41	32	20	27.6	26.3	−1.3
2	85	5	18	61	24	22	30.3	31.1	0.8
3	85	5	18	50	37	21	31.4	31.0	−0.4
4	85	5	18	49	37	21	30.3	30.9	0.6
5	0	94	18	74	38	7	45.2	44.2	−1.0
6	0	94	18	77	38	8	44.9	45.5	0.6
7	0	94	18	75	38	8	44.6	43.7	−0.9
8	0	94	18	71	38	7	41.6	42.6	1.0
9	0	94	21	78	35	8	44.1	44.6	0.5
10	0	94	18	79	35	8	45.0	44.4	−0.6
							Group average		−0.06
							Standard Deviation		0.85
							Sum of squares		6.58
							HLF (cal/min°C)		**150**

and from equation (34.29)

$$T_{\text{air,out}} = \frac{(1166.45\text{g/min})(0.238\,\text{cal/g°C})(70°\text{C}) + 0.8(4\text{g/min})(1.0\ \text{cal/g°C})(22°\text{C})}{(1166.45\text{g/min})(0.238\ \text{cal/g°C}) + 0.8(4\ \text{g/min})(1.0\,\text{cal/g°C}) + 282\,\text{cal/min°C}} + \frac{-0.8(4\text{g/min})(540\ \text{cal/g}) + (282\ \text{cal/min°C})(22°\text{C})}{(1166.45\ \text{g/min})(0.238\ \text{cal/g°C}) + 0.8(4\text{g/min})(1.0\ \text{cal/g°C}) + 282\,\text{cal/min°C}}$$

$T_{\text{air,out}} = 42.6°C$

Based on this result, the inlet air temperature must be higher than 70°C. Increasing the estimate to $T_{\text{air,in}} = 85°\text{C}$ gives

$$m_{\text{air,in}} = 1117.57\,g/\text{min}$$

and

$$T_{\text{air,out}} = 49.3°C$$

This could be iterated further to get an exhaust air temperature closer to 50°C, but this estimate is well within the accuracy of the model and the variability of the actual equipment. Therefore, the inlet air temperature set point required to achieve a target exhaust air temperature of 50°C is approximately 85°C.

(b) To determine the relative humidity of the exhaust air, we need to determine the molar flow rate of water vapor exiting the coater. Based on the material balance for water around the control volume, the molar flow rate of water vapor in the exhaust stream should be equal to amount of water vapor entering in the drying air plus the amount of water added through the coating solution. First, calculate the water vapor partial pressure in the inlet air, which is, by definition, the vapor pressure at the dew point temperature. This can be determined using the Arden Buck equation.

$$P_{\text{w,in}} = P^*_{\text{w}}(@T_{\text{dew}}) = 0.012\,\text{atm}$$

Assuming an ideal gas mixture the mole fraction of water vapor in the inlet stream can be calculated by the ratio of the partial pressure to the total pressure (which is assumed to be atmospheric).

$$y_{\text{w,in}} = \frac{P_{\text{w,in}}}{P_{\text{total}}} = \frac{0.012\ \text{atm}}{1\ \text{atm}} = 0.012$$

and, thus, the mole fraction of dry air is

$$y_{\text{air,in}} = 1 - y_{\text{w,in}} = 0.988$$

The overall molar flow rate of the inlet air stream is the mass flow rate divided by the average molecular weight of the inlet air:

$$\dot{n}_{\text{inlet}} = \frac{m_{\text{air}}}{MW_{\text{inlet}}} = \frac{m_{\text{air}}}{y_{\text{w,in}}MW_w + y_{\text{air,in}}MW_{\text{air}}} = \frac{1117.57\ \text{g/min}}{0.012 \times 18\ \text{g/mol} + 0.988 \times 29\ \text{g/mol}} = 38.713\ \text{mol/min}$$

and the molar flow rate of water vapor in the inlet air is

$$\dot{n}_{\text{w,inlet}} = y_{\text{w,in}} \times \dot{n}_{\text{inlet}} = 0.012 \times 38.713 = 0.4646\ \text{mol/min}$$

The contribution of water vapor from the coating solution is

$$\dot{n}_{\text{w,spray}} = m_{\text{coat}}\left(\frac{x_{\text{w}}}{MW_{\text{w}}}\right) = 4\ \text{g solution/min} \times \left(\frac{0.8\ \text{g Water/g Solution}}{18\ \text{g Water/mol}}\right) = 0.1778\ \text{mol/min}$$

By conservation of mass, the molar flow rate of water vapor in the exhaust air stream is

$$\dot{n}_{\text{w,outlet}} = \dot{n}_{\text{w,inlet}} + \dot{n}_{\text{w,spray}} = 0.4646 + 0.1778 = 0.6424\ \text{mol/min}$$

and the overall molar flow rate of the exhaust air stream is

$$\dot{n}_{\text{outlet}} = \dot{n}_{\text{inlet}} + \dot{n}_{\text{w,spray}} = 38.713 + 0.1778 = 38.891\ \text{mol/min}$$

Finally, the partial pressure and vapor pressure of water in the exhaust air stream can be calculated as follows:

$$\text{P}_{\text{w,out}} = y_{\text{w,out}}P_{\text{total}} = \frac{\dot{n}_{\text{w,outlet}}}{\dot{n}_{\text{outlet}}}P_{\text{total}} = \frac{0.6424\ \text{mol/min}}{38.891\ \text{mol/min}} \times 1\ \text{atm} = 0.0165\ \text{atm}$$

$P^*_w(@T_{\text{air,out}}) = 0.1177\ \text{atm}$

and thus the relativity humidity of the exhaust air stream is

$$\%\text{RH}_{\text{out}} = \frac{P_{\text{w,out}}}{P^*_{\text{w}}(@T_{\text{air,out}})} \times 100\% = \frac{0.0165\ \text{atm}}{0.1177\ \text{atm}} \times 100\% = 14\%.$$

34.3.4.6 Process Scale-Up Based on Model Predictions

An important feature of the thermodynamic film-coating model is in its predictive capabilities, which can be used for process simulation and to assist with scale-up from one film coater to another. Typically, when a film-coating process is scaled to a larger unit it is desirable to maintain the same thermodynamic conditions in the pan that the tablets are exposed to during coating. This can be accomplished by matching the temperature and relative humidity of the exhaust air stream across the two coaters when the HLF for each coater is known. The thermodynamic model can be used to determine the process parameters on the new coater that will result in similar exhaust air conditions to the proven operation of the original coater. Ideally, this will reduce the number of trials required during scale-up and minimize any failed batches during validation.

This concept can be best illustrated through a simple example. Consider a commercial tablet film-coating process that is currently being executed on a Glatt GC-750 model film coater. The heat loss factor for the GC-750 has been determined to be 1080 cal/min°C. The process is well defined on this coater and the proved design space includes inlet air temperatures ranging 60–70°C, spray rates ranging 30–80 g/min, and a drying airflow rate of 300 ft^3/min. The coating is an aqueous formulation consisting of 15 wt% solids. Due to high product demand the commercial site is considering scaling the process to a larger Glatt GC-1000 model film coater, which is typically operated at spray rates ranging 120–250 g/min and a drying airflow rate of 900 ft^3/min. Use the thermodynamic film-coating model to determine the inlet air temperature range in the GC-1000 that will give similar exhaust air temperature and relative humidity across the two coaters.

First, the exhaust air temperature and relative humidity in the GC-750 at each point of the design space conditions outlined above can be calculated using the thermodynamic model. The resulting four data points define the corner points for the operating space of the GC-750 as outlined in Figure 34.19. This operating space represents the proven acceptable range of thermodynamic conditions that will be used for scale-up to the larger coater.

Since the spray rate range and drying airflow are known on the GC-1000, the thermodynamic model can be used directly to calculate inlet air temperature required to match the exhaust air temperature at each of the four points on the GC-750 operating space. Once the exhaust air temperature is known the corresponding relative humidity can be calculated based on the material balance equations. This procedure is similar to the solution of Example 34.3. The resulting predicted exhaust air temperature/relative humidity operating space of the GC-1000, along with the GC-750 operating space for comparison, is shown in Figure 34.20. The input parameters and model predictions for both the GC-750 and the GC-1000 are shown in Table 34.11. According to the model predictions, the inlet air temperature required in the GC-1000

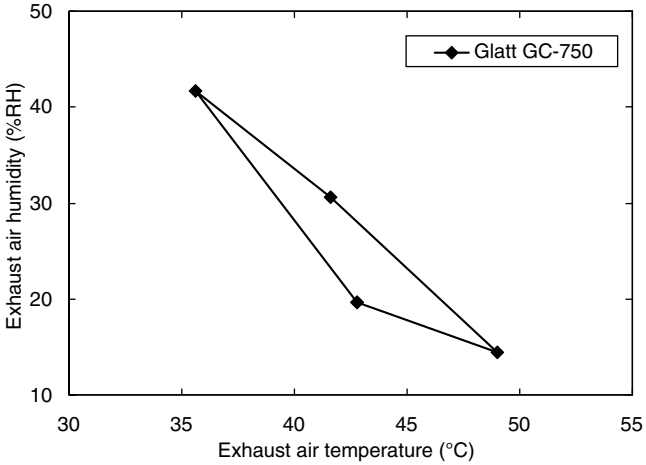

FIGURE 34.19 Exhaust air temperature/relative humidity operating space for the Glatt GC-750 based on inlet air temperatures of 60–70°C, spray rates of 30–80 g/min, and drying airflow rate of 300 ft^3/min.

to match the exhaust air temperature of the GC-750 ranges approximately 57–65°C. It is evident from Figure 34.20 that at these conditions the exhaust air temperature/relative humidity operating space of the GC-1000 matches very well with the proven space of the GC-750.

By matching the thermodynamic conditions across the two coaters we have defined the potential design space for this product on the new coater without running any trials at scale. The operating space can be verified with as many or as few confirmation batches as the operators and formulators deem necessary. We can also map out a design space plot that allows one to visualize the relationship between changes in spray rate, inlet air temperature, and exhaust air temperature

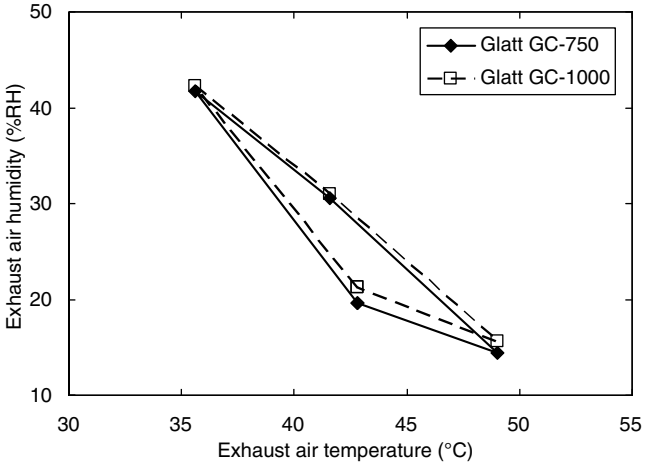

FIGURE 34.20 Exhaust air temperature/relative humidity operating space for the Glatt GC-1000 based on inlet air temperatures of approximately 57–65°C, spray rates of 120–250 g/min, and drying airflow rate of 900 ft^3/min. The GC-750 operating space is shown for comparison.

TABLE 34.11 Operating Conditions and Model Predictions for GC-750/GC-1000 Scale-Up

Glatt GC-750				Glatt GC-1000			
Inlet Temperature (°C)	Spray Rate (g/min)	Exhaust Temperature (°C)	%RH	Inlet Temperature (°C)	Spray Rate (g/min)	Exhaust Temperature (°C)	%RH
60	30	42.8	19.6	56.6	120	42.8	21.3
60	80	35.6	41.7	57	250	35.6	42.3
70	30	49	14.4	64.7	120	49	15.6
70	80	41.6	30.6	65.2	250	41.6	31

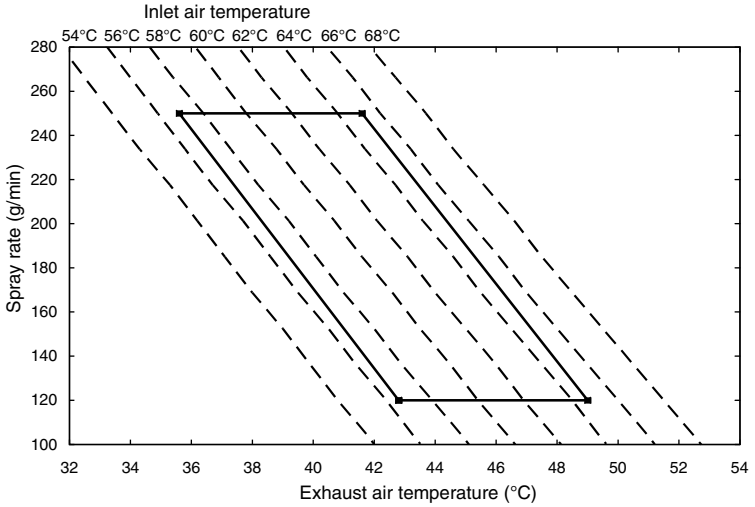

FIGURE 34.21 Design space contour plot for the Glatt GC-1000 film coater for a drying airflow rate of 900 ft^3/min.

for a given drying airflow rate. This type of plot for the GC-1000 film coater is shown in Figure 34.21. The contour plot allows one to map out any combination of operating conditions (inlet air temperature, exhaust air temperature, and spray rate) within the design space for the given drying airflow rate. It also allows operators and formulators to visualize how the exhaust air temperature changes as a function of both spray rate and inlet air temperature across the entire design space.

This exercise has illustrated how the thermodynamic film-coating model can be used to predict specific operating conditions, assist with scale-up from one coater to another, and also simulate different operation scenarios on a given film coater. The model is an extremely versatile predictive tool that is applicable to a wide range of coating formulations on units ranging from lab scale coaters to commercial sized equipment.

34.4 SUMMARY

This chapter highlighted several modeling techniques applied to the design, development, and scale-up for solid oral drug products. These process modeling techniques were discussed and exemplified with case studies ranging from raw material specifications to process parameter predictions in wet granulation and film coating. Specific consideration was given to transfer and scale-up issues along with general process design related challenges to pharmaceutical process R&D. There are many other modeling approaches available to formulation and process scientists that were not covered in this chapter. However, the purpose was to demonstrate that the fundamental principles taught in the chemical engineering curriculum ensure the chemical engineer is well poised to apply and implement modeling techniques to solve challenging issues in the pharmaceutical industry.

REFERENCES

1. Wassgren C, Curtis JS. The application of computational modeling to pharmaceutical materials science. *MRS Bull*. 2006;31(11):900–904.
2. Davidson DL. The enterprise-wide application of computational fluid dynamics in the chemicals industry. 6th World Congress of Chemical Engineering Melbourne, Australia, 2001.

3. Louie AS, Brown MS, Kim A.Measuring the return on modeling and simulation tools in pharmaceutical development. White paper No, HI204892, Health Industry Insights, 2007.
4. Garcia-Munoz S. Establishing multivariate specifications for incoming materials using data from multiple scales. *Chemometr. Intell. Lab. Syst.* 2009;98(1):51–57.
5. Ketterhagen WR. Modeling granular segregation during hopper discharge. 2006.
6. Ketterhagen WR, am Ende MT, Hancock BC. Process modeling in the pharmaceutical industry using the discrete element method. *J. Pharm. Sci.* 2009;98(2):442–470.
7. Ketterhagen WR, Curtis JS, Wassgren CR. Stress results from two-dimensional granular shear flow simulations using various collision models. *Phys. Rev. E* 2005;71(6-1):061307/1–061307/11.
8. Ketterhagen WR, Curtis JS, Wassgren CR, Hancock BC. Modeling granular segregation in flow from quasi-three-dimensional, wedge-shaped hoppers. *Powder Technol*. 2008;179(3):126–143.
9. Ketterhagen WR, Curtis JS, Wassgren CR, Hancock BC. Predicting the flow mode from hoppers using the discrete element method. *Powder Technol*. 2009;195(1):1–10.
10. Ketterhagen WR, Curtis JS, Wassgren CR, Kong A, Narayan PJ, Hancock BC. Granular segregation in discharging cylindrical hoppers: a discrete element and experimental study. *Chem. Eng. Sci.* 2007;62(22):6423–6439.
11. Iveson SM, Litster JD, Hapgood K, Ennis BJ. Nucleation, growth and breakage phenomena in agitated wet granulation processes: a review. *Powder Technol*. 2001;117(1–2):3–39.
12. Bilgili E, Scarlett B. Population balance modeling of nonlinear effects in milling processes. *Powder Technol.* 2005;153(1):59–71.
13. Kremer DM, Hancock BC. Process simulation in the pharmaceutical industry: a review of some basic physical models. *J. Pharm. Sci.* 2006;95(3):517–529.
14. Kunii D, Levenspiel O. *Fluidization Engineering*, Butterworth-Heinemann, Newton, MA, 1991.
15. Bi HT, Ellis N, Abba IA, Grace JR. A state-of-the-art review of gas–solid turbulent fluidization. *Chem. Eng. Sci.* 2000;55(21):4789–4825.
16. Gurson AL. Continuum theory of ductile rupture by void nucleation and growth. Part I. Yield criteria and flow rules for porous ductile media. *J. Eng. Mater. Technol.* 1977;9:2–15.
17. Schofield AN, Wroth CP. *Critical State Soil Mechanics*, McGraw-Hill, London, 1968.
18. DiMaggio FL, Sandler IS. Material model for granular soils. *J. Eng. Mech. Div.* 1971;97:935–950.
19. Drucker DC, Gibson RE, Henkel DJ. Soil mechanics and work hardening theories of plasticity. *Trans. Am. Soc. Civil Eng.* 1957;122:338–346.
20. am Ende MT, Berchielli A. A thermodynamic model for organic and aqueous tablet film coating. *Pharm. Dev. Technol.* 2005;10(1):47–58.
21. Box GEP, Hunter WG, Hunter JS. *Statistics for Experimenters: An Introduction to Design, Data Analysis, and Model Building*, Wiley, 1978.
22. MacGregor JF, Yu H, Garcia Munoz S, Flores-Cerrillo J. Data-based latent variable methods for process analysis, monitoring and control. *Comput. Chem. Eng.* 2005;29(6):1217–1223.
23. Page S, Baumann KH, Kleinebudde P. Mathematical modeling of an aqueous film coating process in a Bohle Lab-Coater. Part 1. Development of the model. *AAPS Pharm. Sci. Tech.* 2006;7(2):42.
24. Page S, Baumann K-H. Mathematical modeling of an aqueous film coating process in a Bohle Lab-Coater. Part 2. Application of the model. *AAPS Pharm. Sci. Tech.* 2006;7(2):43.
25. Stetsko G, Banker GS, Peck GE. Mathematical modeling of an aqueous film coating process. *Pharm. Technol.* 1983;7(11):50, 52–53, 56, 58, 60, 62.
26. Muteki K, MacGregor JF, Multi-block PLS modeling for L-shape data structures with applications to mixture modeling. *Chemometr. Intell. Lab. Syst*. 2007;85:186.
27. Garcia Munoz S, MacGregor JF, Kourti T. Product transfer between sites using Joint-Y PLS. *Chemometr. Intell. Lab. Syst.* 2005;79(1–2):101–114.
28. Garcia-Munoz S, Kourti T, MacGregor JF, Mateos AG, Murphy G. Troubleshooting of an industrial batch process using multivariate methods. *Ind. Eng. Chem. Res.* 2003;42(15):3592–3601.
29. Kourti T, Lee J, MacGregor JF. Experiences with industrial applications of projection methods for multivariate statistical process control. *Comput. Chem. Eng.* 1996; *20S*:S745.
30. Neogi D, Schlags CE. Multivariate statistical analysis of an emulsion batch process. *Ind. Eng. Chem. Res.* 1998;37(10):3971–3979.
31. Garcia-Munoz S, Kourti T, MacGregor, JF, Apruzzese F, Champagne M. Optimization of batch operating policies. Part I. Handling multiple solutions. *Ind. Eng. Chem. Res.* 2006;45(23):7856–7866.
32. Garcia-Munoz S, MacGregor JF, Neogi D, Latshaw BE, Mehta S. Optimization of batch operating policies. Part II. Incorporating process constraints and industrial applications. *Ind. Eng. Chem. Res.* 2008;47(12):4202–4208.
33. Doyle FJ, Harrison CA, Crowley TJ. Hybrid model-based approach to batch-to-batch control of particle size distribution in emulsion polymerization. *Comput. Chem. Eng.* 2003;27:1153–1163.
34. Flores-Cerrillo J, MacGregor JF. Within-batch and batch-to-batch inferential-adaptive control of semi-batch reactors: a partial least squares approach. *Ind. Eng. Chem. Res.* 2003;42(14):3334–3345.
35. Flores-Cerrillo J, MacGregor JF. Latent variable MPC for trajectory tracking in batch processes. *J. Process Control* 2005;15(6):651–663.
36. Bharati MH, Liu JJ, MacGregor JF. Image texture analysis: methods and comparisons. *Chemometr. Intell. Lab. Syst.* 2004;72(1):57–71.
37. Yu H, MacGregor JF. Multivariate image analysis and regression for prediction of coating content and distribution in the production of snack foods. *Chemometr. Intell. Lab. Syst.* 2003;67(2):125–144.

38. Duchesne C, MacGregor JF. Establishing multivariate specification regions for incoming materials. *J. Qual. Technol.* 2004;36(1):78–94.
39. am Ende MT, Blackwood DO, Gierer DS, Neu CP. Challenges in development and scale-up of low dose dry granulation products: a case study. In: Zheng J, editor. *Analytical and Formulation Development For Low-Dose Oral Drug Products*, Wiley, New York, 2009; pp.117–157.
40. U.S. FDA. Draft Guidance for Industry: Quality Systems Approach to Pharmaceutical CGMP Regulations, 2006.
41. U.S. FDA. International Conference on Harmonisation: Guidance on Q8(R1) Pharmaceutical Development. *Fed. Regist.* 2009;74(109):27325–27326.
42. U.S., FDA, International Conference on Harmonisation: Guidance on Q9 Quality Risk Management. *Fed. Regist.* 2006;71(106):32105–32106.
43. U.S. FDA, International Conference on Harmonisation: Guidance on Q10 Pharmaceutical Quality System. *Fed. Regist.* 2009;74(66);15990–15991.
44. Nosal R, Schultz T. PQLI definition of criticality. *J. Pharm. Innov.* 2008;3:79–87.
45. Nomikos P, MacGregor JF. Multivariate SPC charts for monitoring batch processes. *Technometrics* 1995;37(1):41–58.
46. Hertz H. Über die Berührung fester elastischer Körper. *J. Reine Angew. Math.* 1882;92:136.
47. Zhu HP, Zhou ZY, Yang RY, Yu AB. Discrete particle simulation of particulate systems: theoretical developments. *Chem. Eng. Sci.* 2007;62(13):3378–3396.
48. Zhu HP, Zhou ZY, Yang RY, Yu AB. Discrete particle simulation of particulate systems: a review of major applications and findings. *Chem. Eng. Sci.* 2008;63(23):5728–5770.
49. United States Pharmacopeia. Uniformity of dosage units. *Pharmacopeia Forum* 2006;32(6):1653–1659.
50. Johanson JR. Predicting segregation of bimodal particle mixtures using the flow properties of bulk solids. *Pharm. Technol. Europe* 1996;8(1):38–44.
51. Levin M. Wet granulation: end-point determination and scale-up. In: Swarbrick J, editor. *Encyclopedia of Pharmaceutical Technology*, Taylor & Francis, Boca Raton, FL, 2006, pp. 4078–4098.
52. He X, Lunday KA, Li L-C, Sacchetti MJ. Formulation development and process scale up of a high shear wet granulation formulation containing a poorly wettable drug. *J. Pharm. Sci.* 2008;97(12):5274–5289.
53. Bier HP, Leuenberger H, Sucker H. Determination of the uncritical quantity of granulating liquid by power measurements on planetary mixers. *Pharm. Ind.* 1979;41(4);375–380.
54. Leuenberger H. Granulation, new techniques. *Pharma. Acta Helv.* 1982;57(3):72–82.
55. Leuenberger H. New trends in the production of pharmaceutical granules: the classical batch concept and the problem of scale-up. *Eur. J. Pharm. Biopharm.* 2001;52(3):279–288.
56. Leuenberger H, Puchkov M, Krausbauer E, Betz G. Manufacturing pharmaceutical granules: is the granulation end-point a myth? *Powder Technol.* 2009;189(2):141–148.
57. Faure A, Grimsey IM, Rowe RC, York P, Cliff MJ. Applicability of a scale-up methodology for wet granulation processes in Collette Gral high shear mixer-granulators. *Eur. J. Pharm. Sci.* 1999;8(2):85–93.
58. Landin M, York P, Cliff MJ, Rowe RC, Wigmore AJ. Scale-up of a pharmaceutical granulation in fixed bowl mixer-granulators. *Int. J. Pharm.* 1996;133(1–2):127–131.
59. Cunningham JC, Sinka IC, Zavaliangos A. Analysis of tablet compaction. I. Characterization of mechanical behavior of powder and powder/tooling friction. *J. Pharm. Sci.* 2004;93:2022–2039.
60. Han L, Elliott J, Bentham A, Mills A, Amidon G, Hancock B. A modified Drucker–Prager cap model for die compaction simulation of pharmaceutical powders. *Int. J. Solids Struct.* 2008;45(10):3088–3106.
61. Sinka IC. Modelling powder compaction. *KONA* 2007;25:4–22.
62. Sinka IC, Cunningham JC, Zavaliangos A. Analysis of tablet compaction. II. Finite element analysis of density distributions in convex tablets. *J. Pharm. Sci.* 2004;93(8):2040–2053.
63. Sinka IC, Cunningham JC, Zavaliangos A. The effect of wall friction in the compaction of pharmaceutical tablets with curved faces: a validation study of the Drucker–Prager cap model. *Powder Technol.* 2003;133(1–3):33–43.
64. Wu CY, Ruddy OM, Bentham AC, Hancock BC, Best SM, Elliott JA. Modelling the mechanical behaviour of pharmaceutical powders during compaction. *Powder Technology* 2005;152(1–3):107–117.
65. Frenning G. Analysis of pharmaceutical powder compaction using multiplicative hyperelasto-plastic theory. *Powder Technology* 2007;172(2):103–112.
66. Michrafy A, Ringenbacher D, Tchoreloff P. Modeling the compaction behavior of powders: application to pharmaceutical powders. *Powder Technol.* 2002;127(3):257–266.
67. Wu CY, Hancock BC, Mills A, Bentham AC, Best SM, Elliott JA. Numerical and experimental investigation of capping mechanisms during pharmaceutical tablet compaction. *Powder Technol.* 2008;181(2):121–129.
68. Zavaliangos A, Galen S, Cunningham J, Winstead D. Temperature evolution during compaction of pharmaceutical powders. *J. Pharma. Sci.* 2008;97(8):3291–3304.
69. am Ende MT, Herbig SM, Korsmeyer RW, Chidlaw MB. Osmotic drug delivery from asymmetric membrane film-coated dosage forms. In: Wise DL,editor. *Handbook of Pharmaceutical Controlled Release Technology*, Marcel Dekker, Inc., New York, 2000, pp.751–785.
70. Ebey GC. A thermodynamic model for aqueous film-coating. *Pharma. Technol.* 1987;11(4):40–50.
71. Rodriguez L, Grecchi R, et al. Variation of operational parameters and process optimization in aqueous film coating. *Pharm. Technol.* 1996;10:76–86.